

AD-A259 080



AFIT/GA/ENY/92D-12

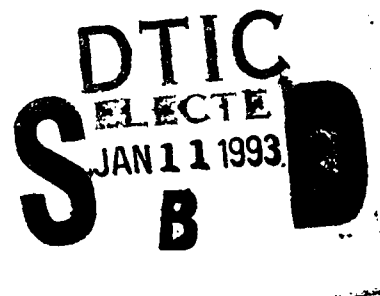
1

POWER ANALYSIS IN FLEXIBLE AUTOMATION

THESIS

Nathan A. Titus
Captain

AFIT/GA/ENY/92D-12



93-00079



98

Approved for public release; distribution unlimited.

98 1 4 21

POWER ANALYSIS IN FLEXIBLE AUTOMATION

THESIS

Presented to the Faculty of the School of Engineering
of the Air Force Institute of Technology
Air University
In Partial Fulfillment of the
Requirements for the Degree of
Master of Science in Astronautical Engineering

Nathan A. Titus, B.S.

Captain

December 15, 1992

Accession For	
NTIS GRA&I	<input checked="checked" type="checkbox"/>
DTIC TAB	<input type="checkbox"/>
Unannounced	<input type="checkbox"/>
Justification	
By	
Distribution/	
Availability Codes	
Dist	Avail and/or Special

Approved for public release; distribution unlimited.

Acknowledgements

I wish to acknowledge the support of my thesis advisor, Dr. Curtis H. Spenny, for his unfailing optimism and invaluable insight. Most of the original work in this thesis was a direct result of our many long discussions. I also would like to thank the other members of my thesis committee, Captain Chris Hall and Dr. Phil Beran, for their many useful comments in the final preparation of this thesis. Finally, my most heartfelt thanks go to my wife, Lori, for her patience, understanding, and encouragement throughout my studies at AFIT.

Nathan A. Titus

Table of Contents

	Page
Acknowledgements	ii
Table of Contents	iii
List of Figures	v
Abstract	viii
I. Introduction	1-1
1.1 Motivation and Goals	1-1
1.2 Scope	1-2
1.3 Thesis Overview	1-2
II. Literature Review	2-1
III. Supporting Theory	3-1
3.1 Screw Theory	3-1
3.1.1 Screw Description	3-1
3.1.2 Screw Coordinate Transformation	3-2
3.1.3 Screw Operations	3-4
3.1.4 Twists and Wrenches	3-7
3.2 Actuator Theory	3-7
3.2.1 DC Motors	3-8
3.2.2 Hydraulic Actuators	3-10
3.3 Manipulator Jacobian	3-15
3.3.1 Velocity Relationship	3-15
3.3.2 Torque Relationship	3-17

	Page
IV. Power Analysis	4-1
4.1 Task Definition	4-1
4.2 Power Analysis	4-4
4.2.1 Output Power	4-4
4.2.2 Power Losses	4-5
4.2.3 Input Power	4-7
4.3 Power Efficiency Metrics	4-14
V. Applications	5-1
5.1 Task/Workspace Planning	5-1
5.2 Actuator Selection	5-6
5.3 Manipulator Structure Selection	5-15
5.4 Kinematic Redundancy	5-19
5.5 Actuator Redundancy Resolution	5-30
VI. Conclusion	6-1
Appendix A. <i>Mathematica</i> Routine Used For Kinematic Redundancy Example	A-1
Bibliography	BIB-1
Vita	VITA-1

List of Figures

Figure	Page
3.1. Screw Coordinate Transformation	3-3
3.2. Relative orientation of two screws.	3-5
3.3. Transforming screws to a common point.	3-6
3.4. Torque-velocity curves for constant voltage in a DC motor.	3-9
3.5. Hydraulic actuator system—piston & spool valve combination.	3-11
3.6. Hydraulic Force-Velocity Curves.	3-14
3.7. A kinematically redundant arm can reach the same position with many joint configurations.	3-16
3.8. Virtual Displacement.	3-17
3.9. Four-Bar Linkage with Redundant Actuator.	3-19
4.1. Task Example.	4-2
4.2. Kinetic Task Example (Lifting).	4-3
4.3. Manipulative Task Example (Moving without a load).	4-3
4.4. Reactive Task Example (Holding a load in a gravity field).	4-4
4.5. Transport Task.	4-6
4.6. Geometric Work.	4-7
4.7. Erasing a Blackboard.	4-8
4.8. Turning a Crank.	4-10
4.9. Planar Grasp.	4-11
5.1. Lift Task.	5-2
5.2. Lift Task Efficiency for Two-Link Serial Arm w/ DC Motors (“El- bow Down”). The lightest region represents $\eta_K \geq 91\%$ and the black region represents $\eta_K \leq 9\%$	5-4

Figure	Page
5.3. "Elbow-Up" and "Elbow-Down" Configurations.	5-5
5.4. Lift Task Efficiency for Two-Link Serial Arm w/ DC Motors ("Elbow Up"). The lightest region represents $\eta_K \geq 91\%$ and the black region represents $\eta_K \leq 9\%$	5-6
5.5. Lift Task in Joint Space for Two-Link Serial Arm.	5-7
5.6. Lift Task Efficiency for Two-Link w/DC Motors. The lightest region represents $\eta_K \geq 91\%$ and the black region represents $\eta_K \leq 9\%$	5-9
5.7. Lift Task Efficiency for Two-Link w/Hydraulic Motors. The lightest region represents $\eta_K \approx 50\%$ and the black region represents $\eta_K \leq 9\%$	5-10
5.8. Hold Task & Slow Transport Task Efficiency for Two-Link w/DC Motors. The lightest region represents $\eta_R \approx 6$ and the black region represents $\eta_R \approx 0$	5-12
5.9. Slow Transport Task Efficiency for Two-Link w/Hydraulic Motors. The lightest region represents $\eta_R \approx 8$ and the black region represents $\eta_R \approx 0$	5-13
5.10. Fast Transport Task Efficiency for Two-Link w/DC Motors. The lightest region represents $\eta_M \approx 650$ and the black region represents $\eta_M \approx 0$	5-14
5.11. Fast Transport Task Efficiency for Two-Link w/Hydraulic Motors. The lightest region represents $\eta_R \approx 0.9$ and the black region represents $\eta_M \approx 0$	5-15
5.12. Kinetic Transport Task Efficiency for Two-Link w/DC Motors. The lightest region represents $\eta_K \approx 95\%$ and the black region represents $\eta_K \leq 9\%$	5-16
5.13. Kinetic Transport Task Efficiency for Two-Link w/Hydraulic Motors. The lightest region represents $\eta_K \approx 40\%$ and the black region represents $\eta_K \leq 5\%$	5-17
5.14. Parallel Type 2-DOF Manipulator.	5-18
5.15. Lift Task Efficiency for 2-DOF Parallel Arm w/DC Motors. The lightest region represents $\eta_K \approx 95\%$ and the black region represents $\eta_K \approx 0\%$	5-19

Figure	Page
5.16. Fast Transport Task Efficiency for 2-DOF Parallel Arm w/DC Motors. The lightest region represents $\eta_K \approx 95\%$ and the black region represents $\eta_K \approx 0\%$	5-20
5.17. Lift Task Efficiency for Two-Link Arm w/DC Motors and $\frac{a_1}{a_2} = 2$. The lightest region represents $\eta_K \approx 95\%$ and the black region represents $\eta_K \approx 0\%$	5-21
5.18. Lift Task Efficiency for Two-Link Arm w/DC Motors and $\frac{a_1}{a_2} = \frac{1}{2}$. The lightest region represents $\eta_K \approx 95\%$ and the black region represents $\eta_K \approx 0\%$	5-22
5.19. Two Possible Joint Configurations for Three-Link Serial Arm. . .	5-23
5.20. Motion of Kinematically Redundant Arm Performing a Lift Task While Optimizing Efficiency.	5-25
5.21. Efficiency of Serial Three-Link During a Lift Task.	5-26
5.22. Motion of Kinematically Redundant Arm Performing a Lift Task While NOT Optimizing Efficiency.	5-26
5.23. Energy Use of Serial Three-Link During a Lift Task. Energy is defined as $E(t) = \int_0^t DP(\tau)d\tau$	5-27
5.24. Task with Redundant Actuation	5-32

Abstract

The performance of an automation or robotic device can be measured in terms of its power efficiency. Screw theory is used to mathematically define the task instantaneously with two screws. The task wrench defines the effect of the device on its environment, and the task twist describes the motion of the device. The tasks can be separated into three task types: kinetic, manipulative, and reactive. Efficiency metrics are developed for each task type. The output power is strictly a function of the task screws, while device input power is shown to be a function of the task, the device Jacobian, and the actuator type. Expressions for input power are developed for two common types of actuators, DC servomotors and hydraulic actuators. Simple examples are used to illustrate how power analysis can be used for task/workspace planning, actuator selection, device configuration design, and redundancy resolution.

POWER ANALYSIS IN FLEXIBLE AUTOMATION

I. Introduction

An underlying cost in all aspects of engineering is the cost of energy. This is particularly true of many automation and robotics applications. In factories, large numbers of robots use power to lift, weld, paint, and grind. In space, possible robotics applications would use energy derived from fuel or equipment which costs thousands of dollars per pound to launch. The energy efficiency of a robot can have a dramatic effect on the economic feasibility of a system, yet this topic is seldom mentioned in robotics and automation literature.

1.1 Motivation and Goals

In order to design and use robots in an energy efficient manner, a basic analysis of their energy use is required. This thesis develops a method to quantify the power efficiency of a robotic mechanism in the completion of a specified task. To this end, the task is defined mathematically using screw theory, and a method is developed that describes the power consumption of the robot in terms of the task. Since the appropriate measure of efficiency of the mechanism depends upon the nature of the required task, several metrics are proposed to cover the spectrum of task possibilities. Finally, the utility of power analysis is illustrated through the use of multiple applications. These include examples of how power analysis can be used for task/workspace planning, actuator selection, manipulator design, and redundancy resolution.

1.2 Scope

The analysis performed in this thesis represents a foundation for an area that has been relatively untouched in robotics. As such, many simplifications have been made in the interest of exploring the substantial opportunities offered by this new approach. First, virtually all of the typical sources of inefficiency have been ignored. The analysis neglects all sources of friction and actuator losses such as motor windage, core-loss, hydraulic fluid leakage, transmission backlash, etc. Another significant limitation is the dependence on the instantaneous definition of the task. With this assumption, a complex function of a robot can be considered the sum of many tasks, each of which is constant. The analysis also neglects dynamic effects on joint torque, instead opting for the quasi-static relationship between joint torques and end-effector loads, which is commonly used in robotics for devices which have little acceleration or for situations where the average joint torques are of interest. Finally, the devices used in the illustrative examples are composed of massless links to ease the computational complexity. These assumptions are not essential to the power analysis, but serve to make this introductory effort more manageable. In the future, it is hoped that refinements can be made to the basic equations established here.

1.3 Thesis Overview

The purpose of Chapter II is twofold. The first purpose is to acquaint the reader with earlier research in the energy efficiency of robots and with the variety of other metrics proposed to aid in robot design and applications. Second, the sources used to provide a basic understanding of screw theory and the workings of robotics actuators are reviewed.

Chapter III lays the foundation for the power analysis. Screw theory is reviewed for use in the task definition, categorization of task types, and the development of an expression for output power. An ideal model for robotics actuators is also presented

which provides a starting point for the incorporation of the actuator into the power analysis.

Chapter IV is the heart of this thesis. There are three primary sections in the chapter. First, it uses screw theory to define the task, and establishes three task types: kinetic, reactive, and manipulative. The analysis relates task type to the relative orientation and magnitude of the task screws. The second section discusses the power in the task. The output power is given in terms of the task screws and the contrast between useful and real power is considered. Several non traditional forms of power loss are illustrated including reactive power and geometric power. Expressions are developed for the device input power for robotic mechanisms using DC motors and hydraulic actuators, and the expressions are transformed from joint space to task space. The third section of the chapter proposes three metrics for power efficiency and describes their relation to task type.

Chapter V contains applications of power analysis and the power efficiency metrics. These examples demonstrate methods for task/workspace planning, actuator comparison, manipulator configuration comparison and redundancy resolution using power analysis.

Chapter VI summarizes the results of Chapters IV and V, and provides conclusions and recommendations for future research.

II. Literature Review

Energy efficiency in robotics has not been well studied. This may be attributed to the relative novelty of the field, since the bulk of research has necessarily been devoted to first understanding the kinematics, dynamics and control of robots. One of the early discussions of energy efficiency was in the context of a walking robot, where Hirose and Umetani in 1980 (1) and Waldron and Kinzel in 1981 (2) discussed one of the advantages of a pantograph geometry as being a high mechanical efficiency. In particular, Waldron mentions "back-driven" actuators as a source of inefficiency in robots.

In 1988, Song and Lee (3) continued the investigation of the mechanical efficiency of pantograph type manipulators. They defined geometric work as the difference between actuator work and output work of a robotic system, and demonstrated that a massless pantograph manipulator does zero geometric work.

Most recently, Spenny and Leahy (4) used the concept of geometric work to define geometric mechanical efficiency (GME). GME was then used to determine the optimum 2-DOF manipulator design for lifting in a gravity field. They considered serial, parallel, and pantograph type manipulators and incorporated the mass of the links into the study. Their results indicated that, in fact, a parallel structure can outperform the pantograph over a significant portion of workspace under these conditions.

Many other metrics have been proposed to define the quality of a manipulator or a grasp. One of the most widely applicable of these is the *measure of manipulability* (MOM) defined by Yoshikawa in 1984 (8). The MOM is a function of the determinant of the Jacobian and its transpose. It is a continuous measure that evaluates the kinematic quality of robotic mechanisms and can be used in design and control of robots. A similar quality measure was suggested by Salisbury and Craig in 1982 (6).

Their metric was the condition number of the Jacobian matrix. In 1991, McArce et. al. (7) applied another similar measure, the determinant of the Jacobian, to the grasping problem. All of these measures can be used to avoid singular configurations of a mechanism, and will find solutions that provide a strong response of the end-effector to the actuators. They can be characterized as "controllability" measures. Another important concept used in redundancy resolution is the potential function. Nakumura (8) provides an excellent demonstration of its application in robotics.

Screw theory has been widely used in robotics literature to illustrate the dynamics of spatial mechanisms. In this thesis, screw theory is an important tool for characterizing the task to be performed by a robotic device. Ball developed much of what is now known as screw theory in 1900, providing a compact notation for force and motion in space. A modern review of screw theory is given by Bottema and Roth (9). In 1978, Hunt (10) demonstrated its applications in kinematic analysis of complex mechanisms. Screw theory has seen significant applications in robotics primarily for grasping theory; see for example, the work of Salisbury and Roth (11) or Holzmann and McCarthy (12).

In 1980, Ohwovoriole extended basic screw theory for use in machine assembly. The 1981 paper by Ohwovoriole and Roth (13), defines the concepts of repelling and contrary screw pairs. These screw pairs complement Ball's reciprocal screw pairs in characterizing contact between rigid bodies. A repelling screw pair implies a loss of contact, contrary screws refer to the penetration of one body by the other, and reciprocal screws are the case for maintaining normal contact. Ohwovoriole also introduces a virtual coefficient for a screw pair and interprets its meaning in the context of a fixed body in contact with a moving body.

Another area of background knowledge important to the understanding of this thesis is actuator design theory. In particular, hydraulic motors and DC motors are considered, since they are the most common types of actuators in modern industrial robots. Snyder (14) and Groover (15) give good basic descriptions of these

actuators in a robotics context. Jones (16) provides more detailed information on the characteristics of DC motors and Hannock (17) clearly explains the principles of electric braking. For a more comprehensive discussion of hydraulics, Watton (18) was a primary source.

III. Supporting Theory

3.1 Screw Theory

Screw theory provides a compact notation for describing force and motion in three-dimensional space. This section is intended as a review of the components and properties of screws. A more comprehensive discussion is given in McCarthy (19) and Hunt (10).

3.1.1 Screw Description A screw represents a line in space that has an associated pitch and magnitude. A useful analogy for interpreting the physical meaning of the components is, not surprisingly, a screw. The centerline of the screw represents the line, the thread pitch (which determines the ratio of linear motion to angular motion) represents the pitch, and the magnitude represents the angle through which the screw is turned. Six independent parameters are required to uniquely define these characteristics. Thus, a screw can be represented by a six-vector of screw coordinates

$$S = (s_1, s_2, s_3, s_4, s_5, s_6) \quad (3.1)$$

or more compactly by two vectors \mathbf{s} and \mathbf{s}_0 as

$$S = (\mathbf{s}, \mathbf{s}_0) \quad (3.2)$$

When the screw is written in standard form, \mathbf{s}_0 is parallel to \mathbf{s} , and can be given as $p\mathbf{s}$, where p is the pitch of the screw.¹ In the coordinates given by equation 3.1, the pitch is

$$p = \frac{s_1 s_4 + s_2 s_5 + s_3 s_6}{s_1^2 + s_2^2 + s_3^2} \quad (3.3)$$

¹When in standard form, generally only four parameters are used to describe the screw. This is because the position of the screw in space is usually obvious from the problem, and a point on the screw axis is chosen as the origin. If a completely arbitrary origin is chosen, the two other parameters are needed to specify a point in space that is on the screw axis.

and in the notation of equation 3.2, it becomes

$$p = \frac{\mathbf{s} \cdot \mathbf{s}_0}{\mathbf{s} \cdot \mathbf{s}} \quad (3.4)$$

The magnitude of the screw is defined as $\|\mathbf{s}\|$, unless $\|\mathbf{s}\| = 0$. In this case, the pitch becomes undefined and then the screw is said to have infinite pitch and a magnitude of $\|\mathbf{s}_0\|$.

3.1.2 Screw Coordinate Transformation As with vectors, when specific components are assigned to a screw, a basis coordinate frame is implied. When the screw is in standard form (i. e. $\mathbf{s}_0 = p\mathbf{s}$), then the origin of the coordinate frame lies on the axis of the screw. Often, however, it is more convenient to describe the screw in a frame that does not have its origin on the screw axis. Screw coordinate transformations provide the means of moving the screw between frames. The transformation can be derived by considering a non-standard screw and computing its equivalent standard form. Suppose

$$S' = (\boldsymbol{\omega}, \mathbf{v}) \quad (3.5)$$

where $\boldsymbol{\omega}$ and \mathbf{v} are not parallel. To put the screw into standard form, the origin of the current frame must be displaced by a vector \mathbf{d} , as shown in Figure 3.1. The transformation is best understood when the components $\boldsymbol{\omega}, \mathbf{v}$ are thought of as the angular velocity and linear velocity of a point on a rigid body. Then it is clear that the displacement \mathbf{d} does not affect the angular rotation and

$$\mathbf{s} = \boldsymbol{\omega} \quad (3.6)$$

The linear velocity is changed by the displacement and becomes

$$\mathbf{s}_0 = \mathbf{v} + \boldsymbol{\omega} \times \mathbf{d} \quad (3.7)$$

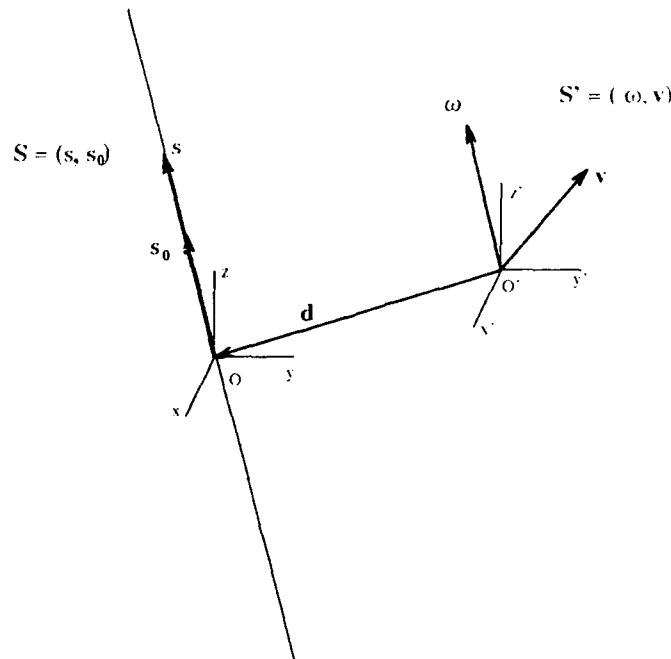


Figure 3.1. Screw Coordinate Transformation

Standard form requires $s_0 = ps = p\omega$, so \mathbf{d} is found by solving

$$p\omega = \mathbf{v} + \omega \times \mathbf{d} \quad (3.8)$$

Cross multiplying both sides by ω , we can solve for \mathbf{d} , and the result is

$$\mathbf{d} = \frac{\omega \times \mathbf{v}}{\omega \cdot \omega} \quad (3.9)$$

Note that the transformation does not change any of the defining characteristics of the screw. The direction and magnitude of the screw are given by the direction of ω , and the pitch is also unchanged as shown below.

$$\begin{aligned} p(S) &= \frac{\mathbf{s} \cdot \mathbf{s}_0}{\mathbf{s} \cdot \mathbf{s}} \\ &= \frac{\omega \cdot (\mathbf{v} + \omega \times \mathbf{d})}{\omega \cdot \omega} \end{aligned}$$

$$\begin{aligned}
&= \frac{\omega \cdot v}{\omega \cdot \omega} \\
&= p(S')
\end{aligned}$$

For a transformation from the standard form to a new frame displaced by $-\mathbf{d}$, equation 3.7 is reversed, giving

$$\mathbf{v} = \mathbf{s}_0 - \omega \times \mathbf{d} \quad (3.10)$$

If the displacement is defined $\mathbf{r} = (-\mathbf{d})$, then the transformation is

$$\mathbf{v} = \mathbf{s}_0 + \omega \times \mathbf{r} \quad (3.11)$$

and

$$\omega = \mathbf{s} \quad (3.12)$$

3.1.3 Screw Operations A useful property of screws is that they can be added vectorially. For two screws $S_1 = (\mathbf{s}_1, \mathbf{s}_{01})$ and $S_2 = (\mathbf{s}_2, \mathbf{s}_{02})$ the result of adding S_1 and S_2 is

$$S = S_1 + S_2 = (\mathbf{s}_1 + \mathbf{s}_2, \mathbf{s}_{01} + \mathbf{s}_{02}) \quad (3.13)$$

This can also be expressed in terms of the screw coordinates, but it is then important that the screws be given in the same frame. If necessary, one screw must be transformed by the procedure described in Section 3.1.2 before the addition can be done.

Another frequently used screw operation is the reciprocal product of screws (13) (12). It is denoted by the "o" operator, and is defined for the two screws S_1, S_2 as

$$S_1 \circ S_2 = \mathbf{s}_1 \cdot \mathbf{s}_{02} + \mathbf{s}_2 \cdot \mathbf{s}_{01} \quad (3.14)$$

When two screws are written in standard form, this product can also be expressed in terms of the geometric relationship of the screws. Given two standard screws in space, there is a distance, d , along a mutually orthogonal line, and a separation angle θ , about this line, as shown in Figure 3.2. In order to perform the reciprocal

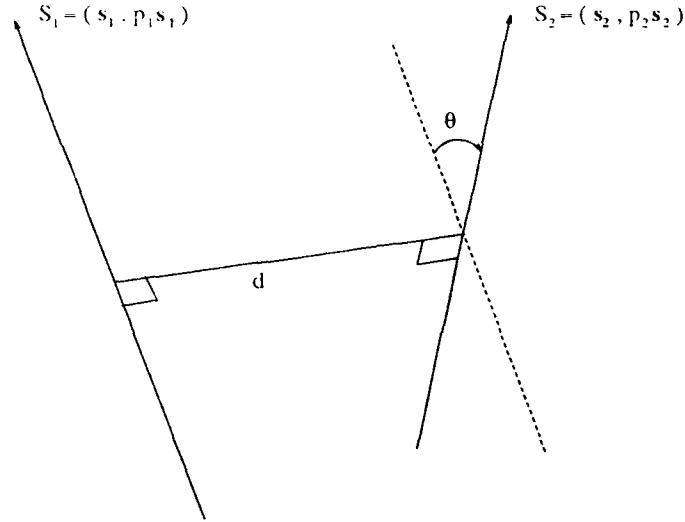


Figure 3.2. Relative orientation of two screws.

product, they must be transformed to a common point C , as shown in Figure 3.3. Then they become

$$S'_1 = (s_1, s_1 \times d_1 + p_1 s_1)$$

$$S'_2 = (s_2, s_2 \times d_2 + p_2 s_2)$$

The reciprocal product is

$$\begin{aligned} r &= S'_1 \circ S'_2 = s_1 \cdot (s_2 \times d_2 + p_2 s_2) + s_2 \cdot (s_1 \times d_1 + p_1 s_1) \\ &= \|s_1\| \|s_2\| (p_1 + p_2) \cos \theta + (s_1 \cdot (s_2 \times d_2) + s_2 \cdot (s_1 \times d_1)) \\ &= \|s_1\| \|s_2\| (p_1 + p_2) \cos \theta + s_1 \cdot ((s_2 \times d_2) + (d_1 \times s_2)) \\ &= \|s_1\| \|s_2\| (p_1 + p_2) \cos \theta + s_1 \cdot (s_2 \times (d_2 - d_1)) \end{aligned}$$

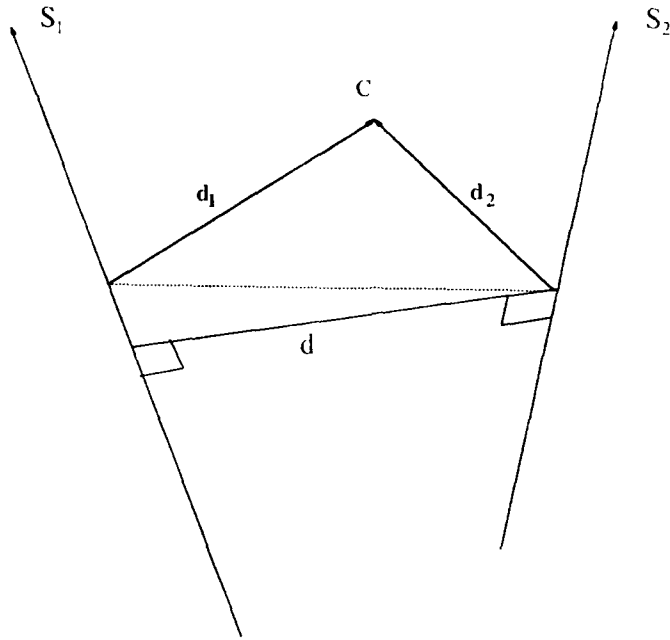


Figure 3.3. Transforming screws to a common point.

$$= \|s_1\| \|s_2\| ((p_1 + p_2) \cos \theta + (d_2 - d_1) \times (s_1 \times s_2))$$

Noting that the mutually orthogonal line is along the unit vector $(s_1 \times s_2) / \|s_1 \times s_2\|$ and that the second term is the projection of the vector $d_2 - d_1$ onto this line, r can be written as

$$r = \|s_1\| \|s_2\| ((p_1 + p_2) \cos \theta - d \sin \theta) \quad (3.15)$$

Equation 3.15 is equivalent to equation 3.14 and can be used when two standard screws are given by their pitch and magnitude rather than by their screw coordinates. The factor $(p_1 + p_2) \cos \theta - d \sin \theta$ contains the information concerning the relative orientation of the two screws and is named the *virtual coefficient* by Ohwovoriole (13).

The reciprocal product and virtual coefficient will be used in chapter IV to help determine task type and output power.

3.1.4 Twists and Wrenches Two special screws are used to describe the dynamics of rigid bodies. These screws are the twist and the wrench.

The twist of a rigid body represents its instantaneous motion. The standard form is written

$$\mathbf{t} = (\boldsymbol{\omega}, p_t \boldsymbol{\omega}) \quad (3.16)$$

and describes the motion in terms of angular velocity about the twist axis and a linear velocity along the axis. In standard form the twist directly describes the motion of all points in the body that lie on the twist axis. In order to describe the motion of other points in the body a screw coordinate transformation must be done. Note that the twist magnitude and direction remain unchanged for all points in the rigid body, so that the angular velocity is constant throughout the body.

The wrench uniquely defines the sum of all external forces and moments on the body. It represents an axis where the forces and moments are aligned and is written

$$\mathbf{w} = (\mathbf{f}, p_w \mathbf{f}) \quad (3.17)$$

Like the twist, the wrench can be applied to any point in space, on or off the body, by the use of the screw coordinate transformation. This is particularly useful, since the wrench may not intersect the physical boundaries of the body when written in standard form. Notice that the direction of the screw axis is independent of the point at which the wrench is described.

3.2 Actuator Theory

Any analysis of power use in robotic devices must eventually lead to the analysis of the device's actuators. This thesis considers the two most common actuators in robotics—DC motors and hydraulic actuators. The discussion of DC motors is based on material found in Jones (16) and Hannock (17), and the primary source of information on hydraulic actuators was Watton (18).

3.2.1 DC Motors Robotic actuators must be able to easily control speed or torque. DC servo-motors are well known for their ability to provide this type of controllability. This section provides the governing equations and torque-speed analysis for a highly idealized DC motor. Three assumptions are made in this analysis. First, only steady-state characteristics are considered, eliminating terms for inductance and armature inertia. Second, inefficiencies due to friction, windage, and core-losses are ignored. Finally, the armature flux is assumed to be constant, as in the case of a permanent magnet motor.

With these restrictions, the voltage equation is

$$V = Ri_a + k_E\omega \quad (3.18)$$

where V is the applied voltage, i_a is the armature current, R is the circuit resistance, ω is the motor speed, and k_E is the motor counter-electromotive force constant. This is often termed the classical motor equation.

The torque developed under the given assumptions is

$$T = k_T i_a \quad (3.19)$$

in which T is generated torque and k_T is the motor torque constant. Combining equations 3.18 and 3.19, current can be eliminated, providing the relation

$$V = \frac{R}{k_T}T + k_E\omega \quad (3.20)$$

or

$$\omega = \frac{V}{k_E} - \frac{R}{k_E k_T}T \quad (3.21)$$

This important equation leads to a useful plot in power analysis, the torque-speed plot. Figure 3.4 shows how the torque and motor speed of equation (3.21) are related for constant levels of control voltage.

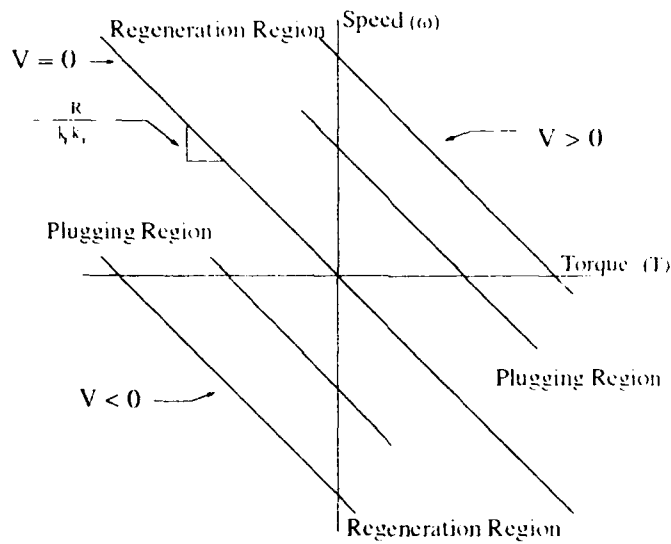


Figure 3.4. Torque-velocity curves for constant voltage in a DC motor.

The last equation relevant to this discussion is the power equation. Motor input power is the product of the voltage and current in the circuit and therefore can be derived from equations 3.18 and 3.19:

$$P = Vi_a = \frac{R}{k_T^2} T^2 + \frac{k_E}{k_T} T \omega \quad (3.22)$$

An examination of this equation reveals several noteworthy points. First, it shows that even when the motor is running at $\omega \approx 0$, or "stall" speed, the power is not zero for a non-zero torque requirement. Next, consider the case of a DC motor called upon to provide a negative torque while running at a positive speed. This condition is known as "electric braking." Equation 3.22 shows that it can result in an input power that is positive, negative or zero. There are three types of electric braking:

1. **Regenerative braking** - In this method, the DC motor is driven backwards, and becomes, in effect, a DC generator. Mechanical energy can be converted into electrical power and returned to the supply.

2. Dynamic braking - The motor acts as a generator in this configuration also, but the generated power is dissipated across a braking resistor, rather than returned to supply. This method is inefficient by design, and also requires a sensing and switching mechanism. It will not be further considered in this thesis.
3. Reverse-current braking - Also known as "plugging", this method reverses the current flow in the motor drawing power from supply to provide the required torque. This power and the mechanical power are eventually dissipated as heat. While plugging is the most inefficient mode of electric braking, if the motor is to be completely flexible in its ability to control speed and torque, then this type of braking cannot always be avoided (i.e., if one wishes to operate the motor over the entire torque-speed plot, then sometimes it will have to plug).

It can be seen in Figure 3.4 that the form of electric braking depends on the instantaneous location on the torque-speed plot. The dividing line is the line of zero voltage. In quadrant II, when above this line, the motor regenerates. When below, the motor is plugging. The relation is flipped in quadrant IV. Obviously, the power is always positive when operating in quadrants I and III. The ratio of constants, $R/(k_E k_T)$, determines how much time is spent regenerating and how much is spent plugging. Since regeneration obviously provides better energy efficiency, one would imagine that the best motor design would be one where this ratio is very small. Unfortunately, this results in poor controllability. To see this, imagine that the slope is near zero. Then for a constant control voltage, a small change in speed would result in a huge change in torque. Typical servomotors have a slope near negative one.

3.2.2 Hydraulic Actuators Hydraulic actuators also find wide use in robotics as a result of their many desirable features. They can be made as either rotary or prismatic (linear) actuators, and have excellent accuracy, frequency response, speed range, and power-to-weight ratio. They can also be operated at stall indefinitely

without damage (14). This section reviews the basic theory of an ideal hydraulic actuator coupled with a typical hydraulic servovalve, as shown in Figure 3.5.

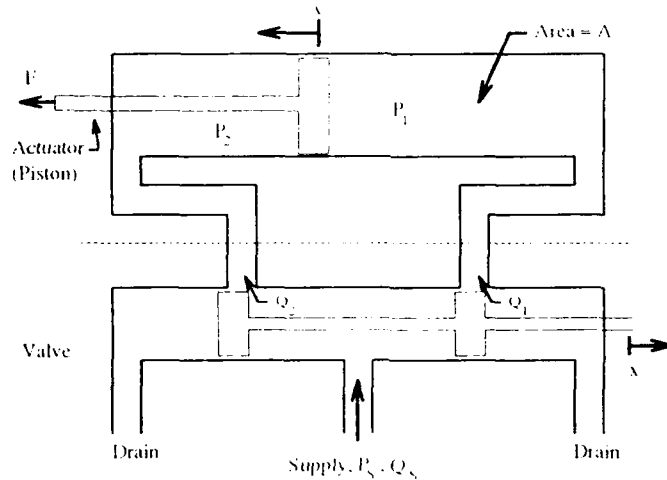


Figure 3.5. Hydraulic actuator system — piston & spool valve combination.

Several assumptions are made in this discussion of an ideal hydraulic system. First, the fluid in the system is considered to be incompressible, and the structure of the system is assumed to be rigid, so that the volumetric flow rate into any section of the flow must equal the flow rate out of the section. This is a good assumption in general, and is often made even in much more rigorous analyses of hydraulics. Second, we assume that there are no flow losses from external leakage or cross-port leakage within the actuator or valve. This is generally adequate for a high level analysis, and it will serve for the purpose of illustrating the potential advantages and disadvantages of hydraulic actuators. It is important to note, however, that leakage due to underlapping² is often desirable in many servovalves, as it improves the control characteristics of the system. Nevertheless, its effects on the overall efficiency of the

²In hydraulics, an *underlapped* spool valve is one where the width of the ports is greater than the width of the spool ends, which allows some flow to get to the actuator even when $x = 0$. When the width of the spool ends are exactly equal to the width of the ports, the valve is called *critically lapped*, and when the spool ends are wider than the actuator ports, the valve is said to be *overlapped*.

system will be considered negligible for our purposes. Finally, the torque losses due to friction will be ignored. This includes viscous friction of the fluid flow, coulomb friction of the machine parts, and a collection of nonlinear friction components, due to hydrodynamic, hydrostatic, and stiction losses. These forces do not change the dominant characteristics that are of interest in this initial study of power use in robotics.

Referring again to the system in Figure 3.5, the ideal piston actuator is modeled by a force equation and a velocity equation:

$$F = (P_1 - P_2)A \quad (3.23)$$

$$Q = Av \quad (3.24)$$

where F is the force applied by the piston, P_1 and P_2 are the pressures in the piston, A is the cross-sectional area of the piston, Q is the volumetric flow rate of the fluid in the piston, and v is the velocity of the piston. The flow rate, Q , is determined by the position of the spool in the valve and the pressure difference across the flow restriction. For flow into the actuator through the upper right port, the rate is given by

$$Q_1 = C_q wx \sqrt{\frac{2(P_s - P_1)}{\rho}}, \quad x > 0 \quad (3.25)$$

which is a form of Bernoulli's pressure/flow equation. In the equation, C_q is the flow coefficient, w is the port width, x is the spool position, and ρ is the fluid density. A similar equation can be written for the flow out of the actuator,

$$Q_2 = C_q wx \sqrt{\frac{2(P_s - P_2)}{\rho}}, \quad x > 0 \quad (3.26)$$

Then, since it is assumed that there is no fluid leakage or compression, $Q = Q_1 = Q_2$. If the drain pressure is negligible, combining equations 3.25 and 3.26 gives the

relations,

$$P_S - P_1 = P_2 \quad (3.27)$$

$$P_S = P_1 + P_2 \quad (3.28)$$

If the load pressure, P_L , is defined by:

$$P_L = P_1 - P_2 \quad (3.29)$$

then

$$P_2 = \frac{1}{2} [(P_1 + P_2) - (P_1 - P_2)] = \frac{1}{2}(P_S - P_L) \quad (3.30)$$

and the flow speed then becomes

$$Q = C_q w x \sqrt{\frac{P_S - P_L}{\rho}} \quad (3.31)$$

Using equations 3.23 and 3.24, the following relation between actuator velocity and actuator force was developed

$$v = \frac{C_q w x}{A \sqrt{\rho}} \sqrt{P_S - \frac{F}{A}} \quad (3.32)$$

Figure 3.6 shows the force-velocity curves for constant x . When linearized, these plots are somewhat analogous to the DC motor torque-speed plot, where x has the same function as the control voltage. However, the large variation in operating speed and force for most robotics applications generally prohibits the use of the linearized equation. An important contrast between the hydraulic actuator and the DC motor is in their operation in the second and fourth quadrants of the force - velocity plots. For DC motors, this is the regime of "electric braking" and power can be either consumed or generated. However, the hydraulic actuator always consumes power when in these quadrants. In a sense, it is "plugging" over the entire second and

fourth quadrants. Although the force-velocity plots are similar, the expression for

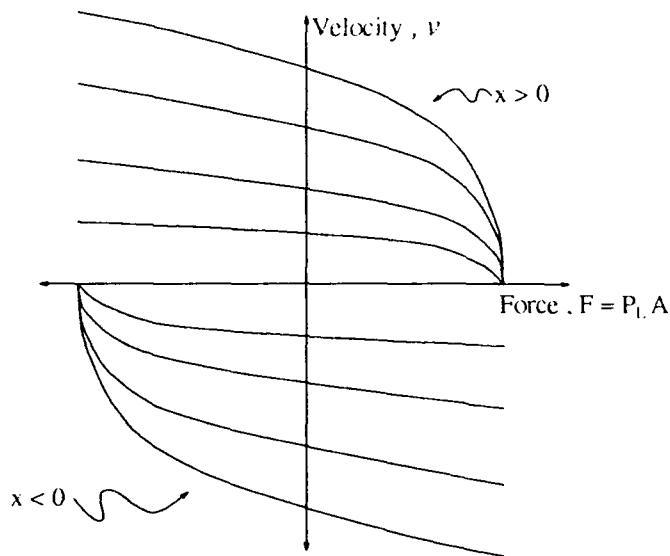


Figure 3.6. Hydraulic Force-Velocity Curves.

hydraulic input power is quite different. The power is the product of the pressure and flow rate supplied to the servovalve by a pump or reservoir. In typical systems, the supply pressure is constant, and the flow speed varies with the load requirements. For the ideal actuator/valve combination, the device input power is

$$DP = P_S Q \quad (3.33)$$

Before writing this in terms of the actuator velocity, consider again the case of a negative force with positive speed. From Figure 3.6, it is evident that this condition implies $x > 0$. Examining Figure 3.5, one finds that $x > 0$ exposes the left side of the piston to the drain port, so no flow returns to the supply. In fact, the flow is still positive out of the supply. Even though the output power is negative, the input power is still positive. The same can be seen for positive force and negative speed.

Therefore, the device power is given by

$$DP = P_S A |v| \quad (3.34)$$

From this equation, it is apparent that when the velocity is zero, the ideal actuator can exert a force without using any power. However, there is also no control over the amount of force exerted, as the generated force is a static reaction force.

3.3 Manipulator Jacobian

In robotics literature, the manipulator Jacobian, J , is well known as the matrix that maps joint velocities to end-effector velocity. The Jacobian can also be used to relate joint torques to end-effector forces for a quasi-static case. Quasi-static is defined in this context as motion that is slow enough that dynamic terms are not significant in the true torque equations.

3.3.1 Velocity Relationship The Jacobian is defined by the equation

$$\dot{\mathbf{x}} = J\dot{\boldsymbol{\theta}} \quad (3.35)$$

in which $\dot{\mathbf{x}}$ is the vector describing the end-effector velocity and $\dot{\boldsymbol{\theta}}$ is the vector containing the velocity of each joint. The elements of the Jacobian are just the partial derivatives of the end-effector position components with respect to the joint angles. For example, element (1,1) of the Jacobian is

$$J_{11} = \frac{\partial x_1}{\partial \theta_1} \quad (3.36)$$

In general, $J = J(\boldsymbol{\theta})$, so that the Jacobian varies over the manipulator workspace. Often the end-effector velocity is known (or its desired velocity is known), and the

joint velocities must be solved for by inverting the Jacobian matrix:

$$\dot{\theta} = J^{-1}\dot{x} \quad (3.37)$$

When the inverse does not exist (for a square J), it is said to be a singularity point of the workspace. When the Jacobian is not square, as is the case when the manipulator has kinematic redundancy (see Figure 3.7), then the general solution for the joint

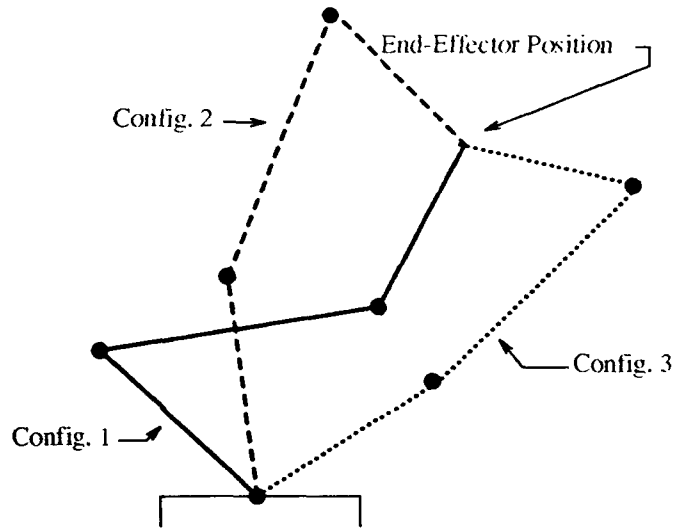


Figure 3.7. A kinematically redundant arm can reach the same position with many joint configurations.

velocities is given by

$$\dot{\theta} = J^{\#}\dot{x} + (I - J^{\#}J)z \quad (3.38)$$

where $J^{\#}$ denotes the pseudoinverse (Moore-Penrose Generalized Inverse) of J and z is an arbitrary vector. Note that multiplying a vector by $(I - J^{\#}J)$ is equivalent to projecting the vector onto the null space of J , so any component of $\dot{\theta}$ created by the second term does not map into end-effector velocity space. The first term, $J^{\#}\dot{x}$, provides the minimum norm solution for $\dot{\theta}$, but the choice of the z vector can be

used when alternate kinematic structures are desired for other reasons, such as task priority or singularity avoidance (8).

3.3.2 Torque Relationship The torque relationship for an open chain mechanism is derived from the Jacobian definition, equation 3.35, and from the principle of virtual work (21). For closed chains, there exists the possibility of actuator redundancy, which can provide an infinite number of solutions for the joint torques.

3.3.2.1 Open-Loop Relationship Consider a force applied to the end of a two-link serial arm as in Figure 3.8. If the end undergoes a virtual displacement

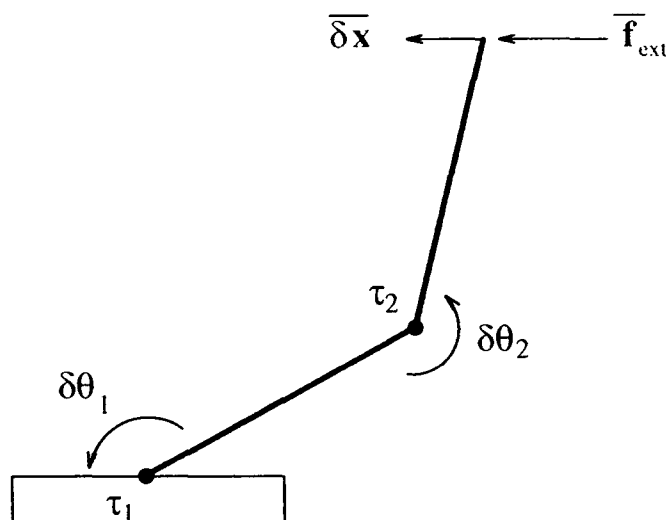


Figure 3.8. Virtual Displacement.

$\delta \mathbf{x}$, then the corresponding displacement of the joints is $\delta \boldsymbol{\theta}$, which is related to $\delta \mathbf{x}$ by equation 3.35, or

$$\delta \mathbf{x} = J \delta \boldsymbol{\theta} \quad (3.39)$$

The total work done by the system is the sum of the work done by the external force and the torque in the joints,

$$\delta W = \mathbf{f}_{\text{ext}}^T \delta \mathbf{x} + \boldsymbol{\tau}^T \delta \boldsymbol{\theta} \quad (3.40)$$

$$\delta W = \mathbf{f}_{ext}^T J \delta \boldsymbol{\theta} + \boldsymbol{\tau}^T \delta \boldsymbol{\theta} \quad (3.41)$$

$$\delta W = (\mathbf{f}_{ext}^T J + \boldsymbol{\tau}^T) \delta \boldsymbol{\theta} \quad (3.42)$$

Since no real work is done, $\delta W = 0$ and since this must hold for all virtual displacements, including $\delta \boldsymbol{\theta} \neq 0$, then

$$0 = \mathbf{f}_{ext}^T J + \boldsymbol{\tau}^T \quad (3.43)$$

$$\boldsymbol{\tau}^T = -\mathbf{f}_{ext}^T J \quad (3.44)$$

$$\boldsymbol{\tau} = -J^T \mathbf{f}_{ext} \quad (3.45)$$

Using the assumed equilibrium condition of the system, the force applied by the manipulator must be equal and opposite to the external force, or $\mathbf{f} = -\mathbf{f}_{ext}$. Then the force applied by the end-effector is related to the torque of the joints by

$$\boldsymbol{\tau} = J^T \mathbf{f} \quad (3.46)$$

3.3.2.2 Actuator Redundancy For open-loop mechanisms, all of the joints must be actuated in order to control the position of the end-effector. However, for closed-loop devices, actuation of all the joints is seldom necessary. When more joints are actuated than is necessary for control, the mechanism is said to have actuator redundancy. Another means by which actuator redundancy can occur is when an open loop mechanism makes contact with the environment. In this instance, kinematic freedom may be lost, but actuator freedom may be gained. Figure 3.9 shows a four-bar mechanism with actuation at two joints. It is well known that the four-bar mechanism only requires one actuated joint to be completely controllable. Therefore the mechanism shown has one redundant actuator. The goal is to express the actuator torques of the closed loop mechanism in terms of the torques required of an open loop mechanism, which can be found by equation 3.46. One method for dealing with actuator redundancy is given by Nakamura in (8).

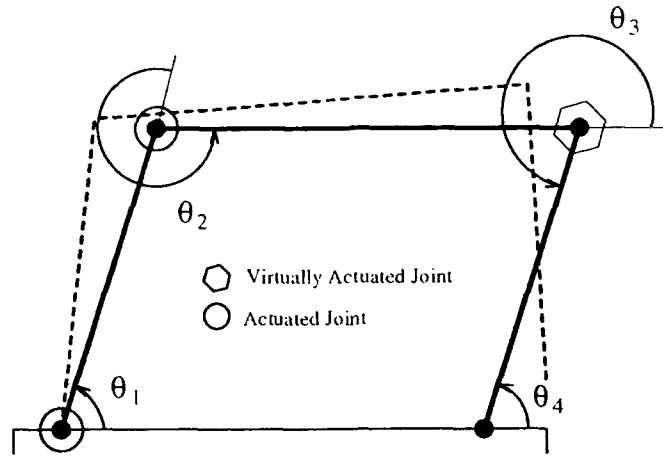


Figure 3.9. Four-Bar Linkage with Redundant Actuator.

First, imagine the mechanism is cut at joint 4. For the new mechanism to be controllable, joint 3 must be actuated, so it is given a virtual actuator. The vector of joint angles, $\theta = \{\theta_1, \theta_2, \theta_3\}$ can be divided into actuated angles $\theta_1 = \{\theta_1, \theta_2\}$ and virtually actuated angles $\theta_2 = \{\theta_3\}$. Now θ_2 can be written as a function of θ_1 .

$$\theta_3 = \pi + \theta_1 \quad (3.47)$$

Then the joint velocities $\dot{\theta}$ can be written

$$\dot{\theta} = G\dot{\theta}_1 \quad (3.48)$$

where

$$G = \begin{bmatrix} I \\ \frac{\partial \theta_2}{\partial \theta_1} \end{bmatrix} = \begin{bmatrix} 1 & 0 \\ 0 & 1 \\ 1 & 0 \end{bmatrix} \quad (3.49)$$

Now express the actuated joints in terms of a basis set of these joints, θ_{10} , where

$$\dot{\theta}_1 = S\dot{\theta}_{10} \quad (3.50)$$

For this example, $\dot{\theta}_{10} = \{\dot{\theta}_1\}$ is a basis set, and

$$S = \begin{bmatrix} 1 \\ -1 \end{bmatrix} \quad (3.51)$$

since $\theta_2 = 2\pi - \theta_1$. Then using virtual work, Nakamura shows that

$$S^T \tau_a = S^T G^T \tau \quad (3.52)$$

where τ_a is the vector of actuated joint torques and τ is the vector of open loop torques, including virtual torques. The general solution to 3.52 is

$$\tau_a = (S^T)^\# S^T G^T \tau + (I - (S^T)^\# S^T) \mathbf{y} \quad (3.53)$$

in which \mathbf{y} is an arbitrary vector. Using a property of pseudoinverses, $(SS^\#)^T = SS^\#$, the equation can be written

$$\tau_a = SS^\# G^T \tau + (I - SS^\#) \mathbf{y} \quad (3.54)$$

Then the vector of open loop torques, τ , can be written in terms of the force applied by the mechanism by using the Jacobian of the virtual open-loop mechanism.

$$\tau = J_v^T \mathbf{f} \quad (3.55)$$

Now the equation becomes

$$\tau_a = SS^\# G^T J_v^T \mathbf{f} + (I - SS^\#) \mathbf{y} \quad (3.56)$$

This provides an expression for torque similar to the expression for velocity in the kinematically redundant case. The first term will counteract external forces while the second, arbitrary, term allows one to vary the internal torque distribution in the

mechanism. The usefulness of actuator redundancy will be studied in greater detail in chapters IV and V.

IV. Power Analysis

4.1 Task Definition

The description of all possible tasks for a robotic device in three-dimensional space is very complex. However, on an instantaneous basis, the task can always be described by the twist of the end-effector or tool and the wrench applied by the tool to the environment. For example, consider a grinding tool on a curved surface, as in Figure 4.1. The task is defined instantaneously by the twist $(\boldsymbol{\omega}, \mathbf{v})$ and wrench (\mathbf{f}, \mathbf{m}) of the tool. These are often initially known (by measurement or estimation) at different points on the body—the figure shows the wrench at point P and the twist at point C . As shown in chapter III, the two screws can be written at a common point. For this example, the point C can be defined as the tool center point (TCP), and at the TCP the twist and wrench would be $(\boldsymbol{\omega}, \mathbf{v})$ and $(\mathbf{f}, (\mathbf{p} - \mathbf{c}) \times \mathbf{f} + \mathbf{m})$, respectively. Hereafter, we define *task* to mean the twist $\mathbf{t} = (\boldsymbol{\omega}, \mathbf{v}_{TCP})$ and wrench $\mathbf{w} = (\mathbf{f}, \mathbf{m}_{TCP})$ at the TCP.

The task can be further characterized by the relative magnitude and orientation of the twist and wrench. All tasks can be divided into three task types: kinetic, reactive, and manipulative. These types are somewhat arbitrary, but some general guidelines for planar tasks are:

- A *kinetic* task is one where the twist and wrench screw axes are parallel and their magnitudes are of the same order.
- A *reactive* task is defined by perpendicular twist and wrench axes and a wrench magnitude much greater than the twist magnitude.
- A *manipulative* task is defined as a task where the twist and wrench axes are perpendicular and the twist magnitude is much greater than the wrench magnitude.

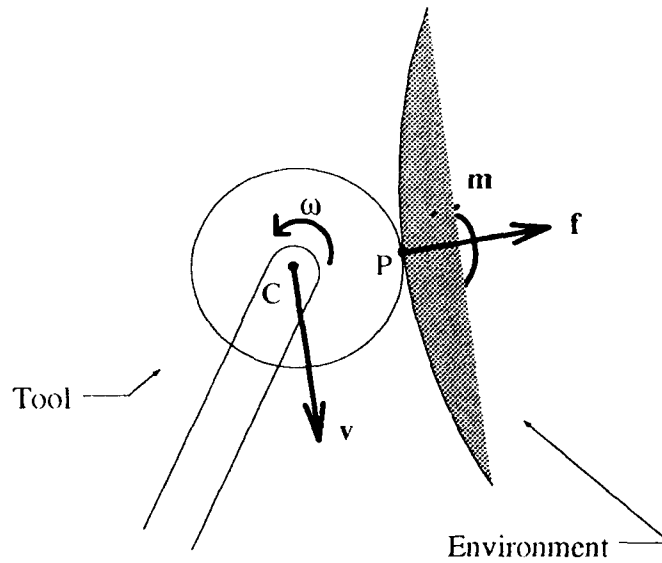


Figure 4.1. Task Example.

Figures 4.2 - 4.4 illustrate these task types. Most real tasks will be a combination of these task types, but can be referred to by the type that they most closely resemble. For example, a task that is dominated by the motion of the end-effector may have a wrench component parallel to the twist, but still would be considered a manipulative task for the purpose of selecting an appropriate metric to measure task accomplishment.

For completely general spatial tasks, the task type is harder to distinguish. One indicator of task type is the virtual coefficient of the twist and wrench, described in chapter III. For a task defined by twist $\mathbf{t} = (\boldsymbol{\omega}, p_t \boldsymbol{\omega})$ and wrench $\mathbf{w} = (\mathbf{f}, p_w \mathbf{f})$, the virtual coefficient is

$$vc = (p_t + p_w) \cos \theta - d \sin \theta \quad (4.1)$$

A kinetic task is defined by $|vc| \gg 0$, while $|vc| \approx 0$ is characteristic of reactive and manipulative tasks. In the latter case, the task screw magnitudes are used to distinguish between reactive and manipulative task types. When the wrench magnitude dominates the twist magnitude, the task is mostly reactive, and when

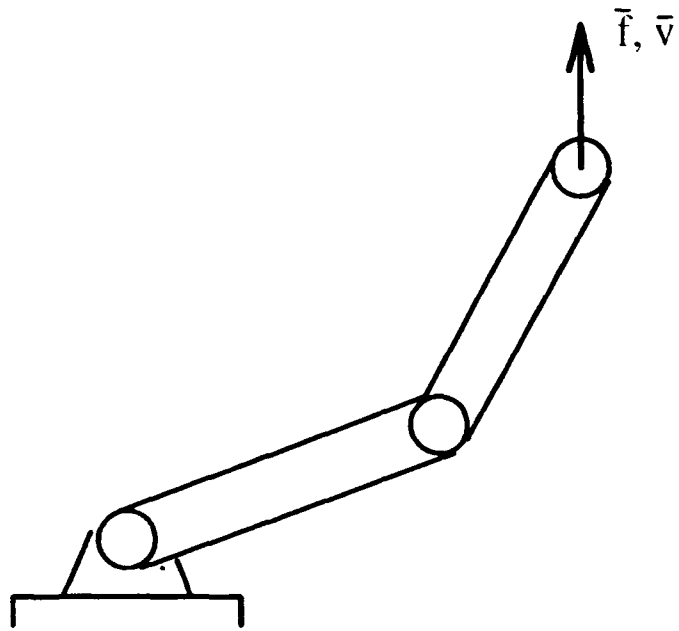


Figure 4.2. Kinetic Task Example (Lifting).

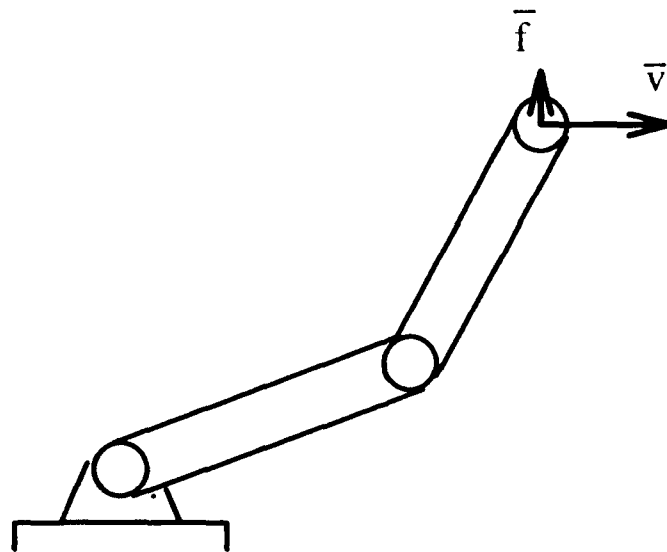


Figure 4.3. Manipulative Task Example (Moving without a load).

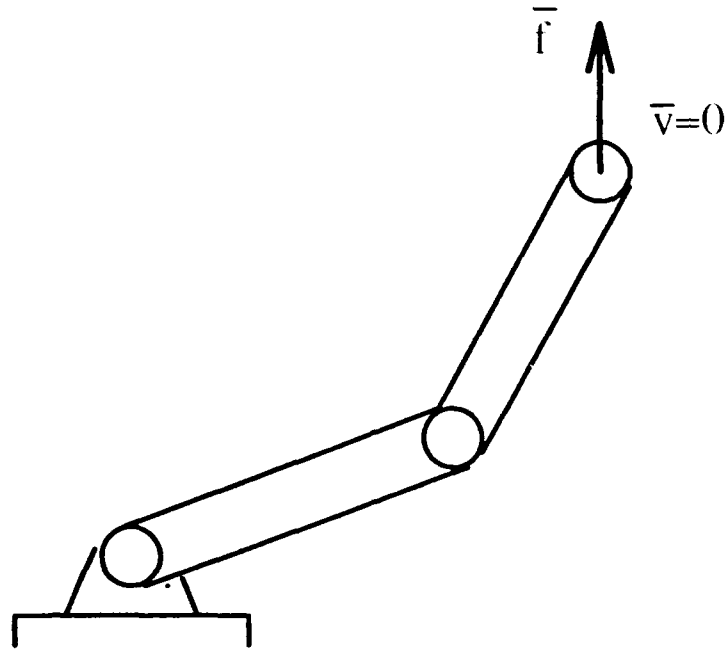


Figure 4.4. Reactive Task Example (Holding a load in a gravity field).

the twist magnitude is largest, the task is mostly manipulative. A more precise definition is not necessary, since the task type is only important in selecting an appropriate metric, and for marginal cases one can simply apply more than one metric and choose the most appropriate result.

4.2 Power Analysis

The power efficiency of a task is generally written in one of the following forms:

$$\eta = \frac{\text{Power Out}}{\text{Power In}} = \frac{\text{Power Out}}{\text{Power Out} + \text{Losses}} = \frac{\text{Power In} - \text{Losses}}{\text{Power In}} \quad (4.2)$$

Each of these elements is examined in the context of a task and robotic device, and where possible, an expression for the power in terms of the task screws is derived.

4.2.1 Output Power Power is defined as the rate at which work is done. Mechanical work is generally defined as the product of a force and the distance

over which the force acts. Using this definition, if the force is constant, power is the product of the force and the velocity. When given the twist and wrench of a robot end effector, the calculation of its output power is a straightforward process of applying the screw reciprocal product. For the task $\mathbf{t} = (\boldsymbol{\omega}, \mathbf{v}_{TCP})$, $\mathbf{w} = (\mathbf{f}, \mathbf{m}_{TCP})$, the reciprocal product is

$$\text{Power Out} = \mathbf{w} \circ \mathbf{t} = \mathbf{f} \cdot \mathbf{v}_{TCP} + \boldsymbol{\omega} \cdot \mathbf{m}_{TCP} \quad (4.3)$$

Obviously, the vector dot product of force and linear velocity summed with the dot product of the moment and angular velocity captures all of the real power delivered by the device to the environment. This expression is useful in that no device specific information is considered—the output power depends only on the given task.

This definition is satisfactory for many important tasks, such as lifting an object in a gravity field, or sliding an object across a rough surface. However, the function of a machine does not always produce an output which can be measured in terms of real power. Consider the task of moving an object horizontally in a gravity field, as shown in Figure 4.5. For this case, the real power out is zero, which would lead typical efficiency metrics to calculate a zero efficiency in completing the task. Yet the input power is not wasted, since a useful job was done. The power provided to the actuators to counter gravity is termed “reactive” power and depends on the actuator type and the geometry of the mechanism. This example demonstrates that the output quantity used in an efficiency metric need not be real power, but may be whatever quantity one considers to be “useful.”

4.2.2 Power Losses Power losses are most often attributed to nonconservative processes such as friction, motor windage, transmission backlash, etc. These types of inefficiencies are well modeled (if not always well-understood) through the use of experimental evidence, and are more appropriately the domain of the actuator engineer. This paper assumes nearly ideal actuators in order to highlight two other

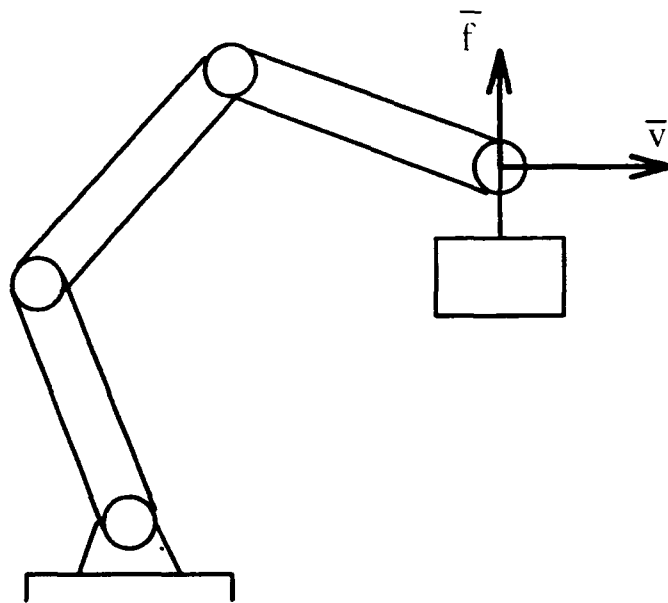


Figure 4.5. Transport Task.

types of losses peculiar to robot-like mechanisms. These losses are the result of 1) actuators working against each other; and 2) actuators working against a stationary environment.

The first loss has been described as “backwork” (3) or “geometric work” (4). An illustration of how actuators can work against each other is given in Figure 4.6. The task is lifting an end load in a gravity field by a two-link serial arm. To produce a change in height of Δy , the actuators must move the joints through incremental displacements of $\Delta\theta_1$ and $\Delta\theta_2$. If the result of each of these displacements is examined serially, instead of simultaneously, it is seen that $\Delta\theta_1$ carries the load above the required height, while $\Delta\theta_2$ lowers the load to correct the deviation. This indicates that the first change requires power exceeding the output power, and the second change produces power equivalent to the excess needed in the first change. However, if the actuators require positive power to drive both rotations, the sum of the actuator power would exceed the real output power. The difference between the input

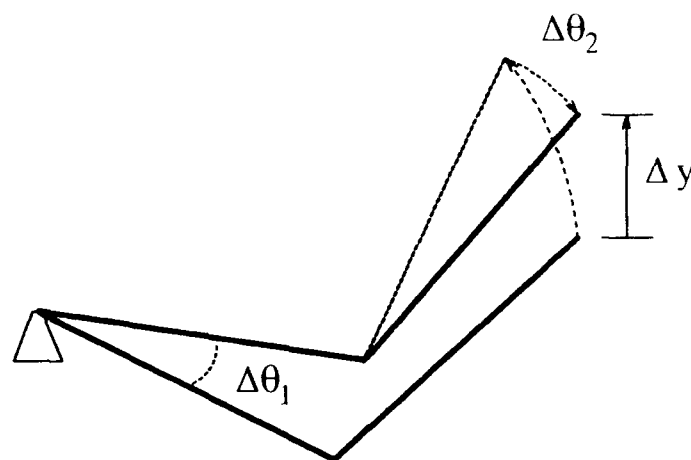


Figure 4.6. Geometric Work.

and output is termed *geometric power*. Geometric power is a loss that depends on the configuration of the device, actuator type, and the assigned task.

The second loss is described as the effect of working against a stationary environment. Suppose the task is erasing a blackboard, as shown in Figure 4.7. While actuator power is required to overcome friction in moving the eraser across the board, power is also used in pressing the eraser against the surface. The power used to generate this normal force is termed “reactive” power. Beyond a required minimum, the normal force is unnecessary for task accomplishment, and hence the reactive power is wasted. Note that this is the same type of power referred to in section 4.2.1 as an alternate output power. In fact, whether reactive power is a loss is entirely dependent upon the task designer’s point of view. Like geometric power, reactive power loss is also dependent on both the device configuration and the task.

4.2.3 Input Power The subtle nature of the geometric and reactive losses makes it difficult to provide an expression for them directly. Therefore the best approach is to add together the power required by each actuator to create the total input power or “device” power. Then the device power can be expressed in terms of

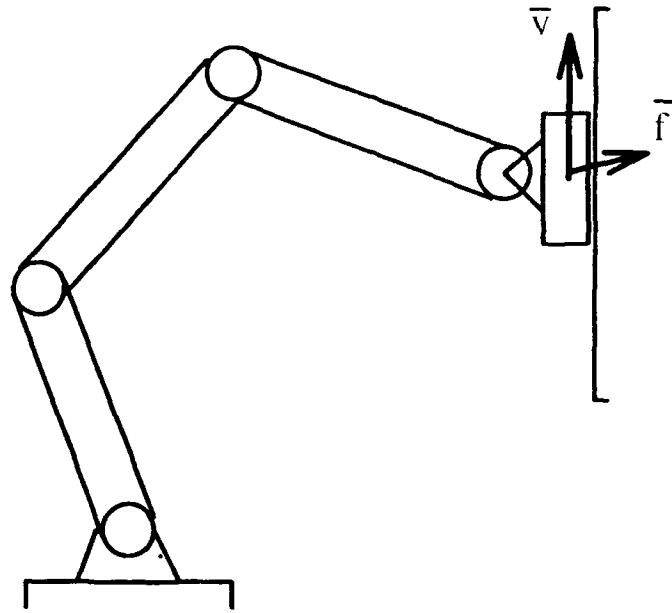


Figure 4.7. Erasing a Blackboard.

the task and efficiency can be found as the ratio of power output (or other quantity) to power input, bypassing the need for the direct formulation of the losses.

Using this approach, an equation for device power of a robot with n actuators is

$$DP = \sum_{i=1}^n DP_i \quad (4.4)$$

where DP_i is the input power of the i^{th} actuator. For now, assume that DP_i is a known function of the torque and velocity required of the actuator, or $DP_i = DP_i(\tau_i, \dot{\theta}_i)$. Then if torque and velocity vectors are defined by

$$\boldsymbol{\tau} = (\tau_1, \tau_2, \dots, \tau_i)$$

$$\dot{\boldsymbol{\theta}} = (\dot{\theta}_1, \dot{\theta}_2, \dots, \dot{\theta}_i)$$

then the total device power becomes a function of these vectors, $DP = DP(\boldsymbol{\tau}, \dot{\boldsymbol{\theta}})$.

Now the description of device power in terms of the original task twist, \mathbf{t} , and wrench, \mathbf{w} , can be derived by transforming the vectors from joint space to task space. This is done through the use of the manipulator Jacobian, as shown in section 3.3. Equation 3.35 can be used to relate $\dot{\boldsymbol{\theta}}$ to \mathbf{t} . However, since the standard Jacobian in robotics literature gives rotational information in the bottom three rows, and the standard twist has the angular velocity as the first three components, a transformation matrix, T , must be added. Then the equation becomes

$$T\mathbf{t} = J\dot{\boldsymbol{\theta}} \quad (4.5)$$

where the T matrix is defined by

$$T = \left[\begin{array}{ccc|ccc} 0 & 0 & 0 & 1 & 0 & 0 \\ 0 & 0 & 0 & 0 & 1 & 0 \\ 0 & 0 & 0 & 0 & 0 & 1 \\ \hline --- & --- & --- & --- & --- & --- \\ 1 & 0 & 0 & 0 & 0 & 0 \\ 0 & 1 & 0 & 0 & 0 & 0 \\ 0 & 0 & 1 & 0 & 0 & 0 \end{array} \right] \quad (4.6)$$

Then the mapping from joint space to task space is given by

$$\dot{\boldsymbol{\theta}} = J^{-1}T\mathbf{t} \quad (4.7)$$

when the robot is not kinematically redundant. If it is redundant, then the expanded form

$$\dot{\boldsymbol{\theta}} = J^\#T\mathbf{t} + (I - J^\#J)\mathbf{z} \quad (4.8)$$

can be used.

Similarly, the joint torques are related to the wrench by¹

$$\boldsymbol{\tau} = \mathbf{J}^T \mathbf{w} \quad (4.9)$$

when the robot does not have actuator redundancy. If actuator redundancy does exist, then the torque equation must be modified to allow for the choice of torque distribution over the actuators, as shown in section 3.3.2.2.

Actuator redundancy only occurs for closed loop mechanisms, but often open link robots will behave as a closed loop when in contact with the environment. Consider a two link arm turning a crank, shown in Figure 4.8. Although the robot

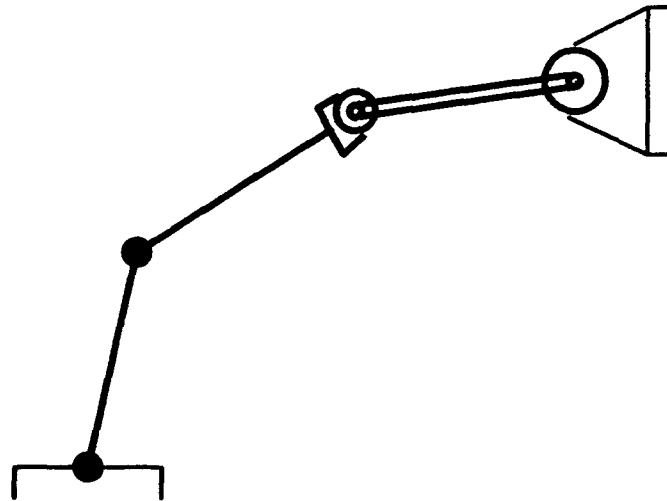


Figure 4.8. Turning a Crank.

is an open loop serial arm, if the end in contact with the crank can be considered a pinned joint, then the robot gains actuator redundancy. In such cases, the open loop torques obtained from equation 4.9 would represent only one of the possible

¹No transformation matrix is needed here, since the moment component of \mathbf{w} is given by its last three elements.

solutions. The general solution is

$$\tau_a = SS^{\#}G^T J^T \mathbf{w} + (I - SS^{\#})\mathbf{y} \quad (4.10)$$

This procedure is also applicable to grasping an object with multiple fingers, since the combination of the fingers and object form a closed chain, as shown in Figure 4.9. The arbitrary term in equation 4.10 is then directly related to the

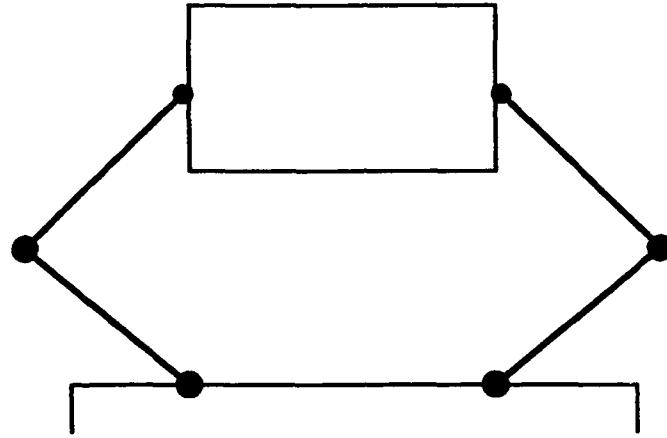


Figure 4.9. Planar Grasp.

internal force of the object.

In the preceding discussion, it was assumed that the device power of each actuator was known as a function of its torque and velocity, so that the total device power could be written as a function of the task screws by combining equation 4.4 with the appropriate joint velocity equation (4.7 or 4.8) and joint torque equation (4.9 or 4.10). In order to determine the actual functions $DP_i(\boldsymbol{\tau}, \dot{\boldsymbol{\theta}})$, the model for the actuator type must be used. For DC motors, the input power is given by equation 3.22,

$$P = \frac{R}{k_T^2} \tau^2 + \frac{k_E}{k_T} \tau \omega$$

Substituting this into equation 4.4, the device power for a DC motor driven robot is²

$$DP = \sum_{i=1}^n \frac{R}{k_T^2} \tau_i^2 + \frac{k_E}{k_I} \tau_i \omega_i \quad (4.11)$$

If the robot has no redundancy, then this can be written in terms of the task screws by using equations 4.7 and 4.9:

$$DP = \frac{R}{k_T^2} (\mathbf{w}^T J J^T \mathbf{w}) + \frac{k_E}{k_T} (\mathbf{w}^T T \mathbf{t}) \quad (4.12)$$

When the mechanism is redundant, the more general equations should be used. These equations are given below.

Kinematic Redundancy

$$DP = \frac{R}{k_T^2} (\mathbf{w}^T J J^T \mathbf{w}) + \frac{k_E}{k_T} (\mathbf{w}^T T \mathbf{t}) \quad (4.13)$$

Actuator Redundancy

$$\begin{aligned} DP = & \frac{R}{k_T^2} [\mathbf{w}^T J G S S^{\#} G^T J^T \mathbf{w} + \mathbf{y}^T (I - S S^{\#}) \mathbf{y}] \\ & + \frac{k_E}{k_T} [\mathbf{w}^T J G S S^{\#} J^{-1} T \mathbf{t} + \mathbf{y}^T (I - S S^{\#}) J^{-1} T \mathbf{t}] \end{aligned} \quad (4.14)$$

Kinematic and Actuator Redundancy

$$\begin{aligned} DP = & \frac{R}{k_T^2} [\mathbf{w}^T J G S S^{\#} G^T J^T \mathbf{w} + \mathbf{y}^T (I - S S^{\#}) \mathbf{y}] \\ & + \frac{k_E}{k_T} [\mathbf{w}^T J G S S^{\#} J^{\#} T \mathbf{t} + \mathbf{y}^T (I - S S^{\#}) J^{-1} T \mathbf{t} \\ & + \mathbf{w}^T J G S S^{\#} (I - J^{\#} J) \mathbf{z} + \mathbf{y}^T (I - S S^{\#}) (I - J^{\#} J) \mathbf{z}] \end{aligned} \quad (4.15)$$

²This assumes that all of the motors have the same motor constants.

Notice that for the case of the simple kinematic redundancy, the arbitrary vector \mathbf{z} is not present. The physical interpretation of this is that for DC motors, when the redundancy is used to change the joint velocities a decrease in input power for one actuator exactly matches the increase in another actuator. Hence, the total device power is constant for a given configuration and task regardless of how the joint velocities are distributed. This does not eliminate the usefulness of power analysis in the resolution of kinematic redundancy, as will be shown in section 5.4.³

When hydraulic actuators are substituted for the DC motors, the device power equations have a significantly different character, due to the difference in how the hydraulics make use of power. The hydraulic actuator power is given by equation 3.33:

$$DP = P_S Q$$

This equation can be rewritten for hydraulic motors using the substitution

$$Q = D_\omega |\dot{\theta}| \quad (4.16)$$

in which D_ω is a motor constant that represents the volumetric displacement of fluid in the motor per radian of angular movement. It is analogous to the cross-sectional area, A , in the piston actuator. Then device power for a motor is

$$DP = P_S D_\omega |\dot{\theta}| \quad (4.17)$$

Substituting this into equation 4.4, the device power for a hydraulic motor actuated robot is

$$DP = \sum_{i=1}^n P_S D_\omega |\dot{\theta}_i| \quad (4.18)$$

Then in terms of the task twist, device power is

³In combination with actuation redundancy, \mathbf{z} does appear, because then the choice of joint torques can affect the balance of power that exists when the redundancy is purely kinematic.

Non-Redundant

$$DP = P_S D_\omega \mathbf{n}^T |J^{-1} T \mathbf{t}| \quad (4.19)$$

Kinematic Redundancy

$$DP = P_S D_\omega \mathbf{n}^T |J^\# T \mathbf{t} + (I - J^\# J) \mathbf{z}| \quad (4.20)$$

in which \mathbf{n} is a vector of ones, $\mathbf{n} = \{1, 1, \dots, 1\}$ and $|\{vector\}|$ indicates a vector comprised of the absolute values of the elements of $\{vector\}$. The equation for the kinematically redundant case shows that the arbitrary choice of joint velocity distribution can have a direct effect on device power, in contrast to the DC motor case. However, actuator redundancy does not have any direct effect, since the power is not a function of the task wrench.

Although there is no direct method of minimizing device power for the actuator redundant case, there are benefits to making the proper choice of torque distribution in the redundant case. Consider the efficiency of a single hydraulic motor

$$\eta = \frac{P_{out}}{P_{in}} = \frac{\tau \dot{\theta}}{P_S Q} = \frac{D_\omega P_L \dot{\theta}}{P_S D_\omega |\dot{\theta}|} = \pm \frac{P_L}{P_S} \quad (4.21)$$

When $\dot{\theta} > 0$, then the actuator efficiency is maximized by letting the torque requirement approach the maximum torque, $P_L \rightarrow P_S$. When $\dot{\theta} < 0$, the least wasted power is attained by minimizing the torque requirement, $P_L \rightarrow 0$. If this principle could be incorporated into the control scheme, then the actuator redundancy might be used to achieve a better overall efficiency.

4.3 Power Efficiency Metrics

In order to use the preceding analysis effectively in robot design, task planning, or joint control, an efficiency metric is required. The type of metric appropriate to a task is often dependent on the task itself. For example, when designing an airplane

for extended range, top speed may be relevant, but it is not the best indicator of how far the plane can fly. The same appears to be true in this analysis. As noted earlier, when the standard measure of efficiency is used for a reactive task, a low result occurs even though the job may be completed in the most efficient way possible. Therefore, three different metrics are proposed, one for each of the three task types.

For kinetic tasks, the familiar efficiency measure is appropriate. Kinetic efficiency is defined as

$$\eta_K = \frac{\text{Output Power}}{\text{Input Power}} = \frac{\mathbf{w} \cdot \mathbf{t}}{DP} \quad (4.22)$$

in which the output power is the reciprocal product of the task screws as defined in section 4.2.1, and DP is the appropriate device input power for the task and actuator type.

For reactive tasks, the reactive efficiency is given by

$$\eta_R = \frac{\text{wrench magnitude}}{\text{Input Power}} = \frac{\|\mathbf{w}\|}{DP} \quad (4.23)$$

where the wrench magnitude, $\|\mathbf{w}\|$, is given by the standard Euclidean norm for a 6-vector.

For manipulative tasks, the efficiency is defined

$$\eta_M = \frac{\|\mathbf{t}\|}{DP} \quad (4.24)$$

where $\|\mathbf{t}\|$ and DP are given in the same manner as for the other metrics. The reactive and manipulative efficiencies represent the ratio of the size of the significant output of the task to the output power. They will not result in a standard efficiency in the range 0% - 100%, but higher values of the metric clearly indicate more efficient use of the power. The measures are analogous to a standard metric for automobiles, miles per gallon. Miles travelled represent the magnitude of the motion, and gallons

are a measure of the energy required to complete the trip. When integrated over a path, η_M would be a nearly identical metric.

V. Applications

Power efficiency can be used in a wide variety of ways in robotics. To demonstrate the range of possibilities, a few simple examples will illustrate the use of power analysis in five areas:

1. Task/Workspace Planning
2. Actuator Selection
3. Manipulator Kinematic Structure Selection
4. Kinematic Redundancy Resolution
5. Actuator Redundancy Resolution

5.1 Task/Workspace Planning

Consider a two-link serial manipulator, driven by DC motors, performing the open loop task of lifting a load in a gravity field (see Figure 5.1). The task screws for this planar task degenerate into vectors,

$$\mathbf{w} = \mathbf{f} = (f_x, f_y)^T \quad (5.1)$$

$$\mathbf{t} = \mathbf{v} = (v_x, v_y)^T \quad (5.2)$$

Since the lifting task has collinear force and velocity (they are both vertical), it is a kinetic task. Then the appropriate metric is the kinetic efficiency given by equation 4.22,

$$\eta_K = \frac{\mathbf{w} \circ \mathbf{t}}{DP}$$

The output power is (for this task, $f_x = v_x = 0$)

$$\mathbf{w} \circ \mathbf{t} = \mathbf{f} \cdot \mathbf{v} = f_y v_y \quad (5.3)$$

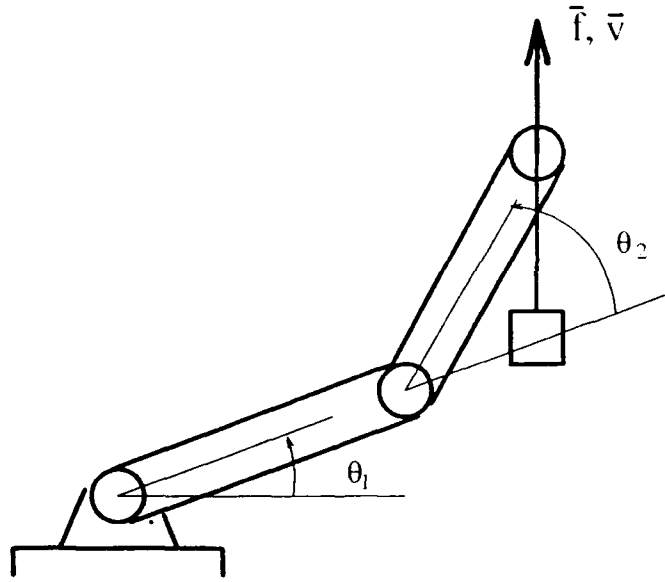


Figure 5.1. Lift Task.

And the device input power for a non-redundant DC motor driven robot is given by equation 4.12

$$DP = \frac{R}{k_T^2} (\mathbf{f}^T J J^T \mathbf{f}) + \frac{k_E}{k_T} (\mathbf{f}^T \mathbf{v})$$

The manipulator Jacobian for a two-link is

$$J = \begin{bmatrix} -a_1 s_1 - a_2 s_{12} & -a_2 s_{12} \\ a_1 c_1 - a_2 c_{12} & -a_2 c_{12} \end{bmatrix} \quad (5.1)$$

in which a_1, a_2 are the link lengths, and sines and cosines of the joint angles are represented by the notation $\sin \theta_1 = s_1$, $\sin(\theta_1 + \theta_2) = s_{12}$.

Since device power is a function of J , and J is a function of position, it is apparent that $DP = DP(x, y)$ for a fixed task. Then one method of optimizing power efficiency is to find the best location for the task relative to the base of the arm.

This optimum location could be found by a number of means, but the simplest method for showing the effect of location on efficiency is a contour plot of the efficiency. This type of plot allows the engineer to quickly identify the best operating regions for robot-task combination.

To provide numerical results, the task was modeled by defining $f_y = 11\text{lb}$, $v_y = 1\text{fps}$ ¹, and the robot was modeled as having link lengths of $a_1 = a_2 = 0.5\text{ft}$ and typical DC motors for actuators. The motors' constants are:

$$\begin{aligned} k_T &= 54\text{oz-in/A} \\ &= 0.28125\text{ft-lb/A} \\ k_E &= 40\text{V/krpm} \\ &= 0.3820\text{V/rad/sec} \\ R &= 0.5\Omega \end{aligned}$$

The efficiency is shown for the first quadrant workspace in Figure 5.2. For this plot, the inverse kinematic equations generate the "elbow down" solution for the joint angles. The lightest regions represent an efficiency of 91% or greater, while the black regions represent an efficiency of less than 9%. The white regions are out of the reachable workspace, which is bounded by the circle $x^2 + y^2 = 1$. The rough edges are the result of the resolution of the plotting method, and do not indicate any real phenomenon. While the plot was designed to show the power efficiency for an instantaneous lift task at different points in workspace, it is also useful to note that one can use it to determine the average efficiency in lifting a specified distance as well. For any *vertical* line drawn on this plot, the total energy expended in lifting a load at *constant* speed along the line could be found by integrating the efficiency along the line and then multiplying by the total output work ($mg\Delta h$). There are several conclusions that one can draw from an examination of this plot.

¹This is the equivalent of 0.745 watts of output power.

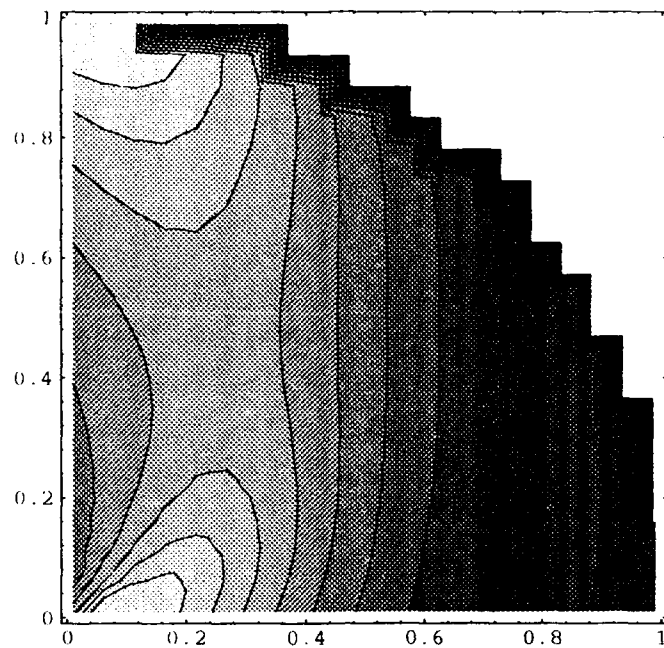


Figure 5.2. Lift Task Efficiency for Two-Link Serial Arm w/ DC Motors ("Elbow Down"). The lightest region represents $\eta_K \geq 91\%$ and the black region represents $\eta_K \leq 9\%$.

First, as one would expect, the efficiency drops off to zero as the edge of reachable workspace is approached. Very large joint speeds and torques are required for small motions and loads in this region, and at the very edge, a degree of freedom is lost. At full extension, ($\theta_2 = 0^\circ$), it is impossible to move up along a vertical path. It is therefore reasonable that the efficiency should decrease as this condition is approached. Second, the efficiency generally improves as the x -position decreases. This is indicative of the reduction in the torque requirements at each joint as the load moves closer to the arms base at $(x, y) = (0, 0)$. One intuitively expects this, since the moment arm is shorter. The efficiency then increases as the joint torques decrease, because the device power is a strong function of the joint torques.

Aside from optimum location, there is another option that a planner could consider. This is the choice of the "elbow up" or "elbow down" configuration for

the arm (see figure 5.3). While space and mounting considerations may dictate this

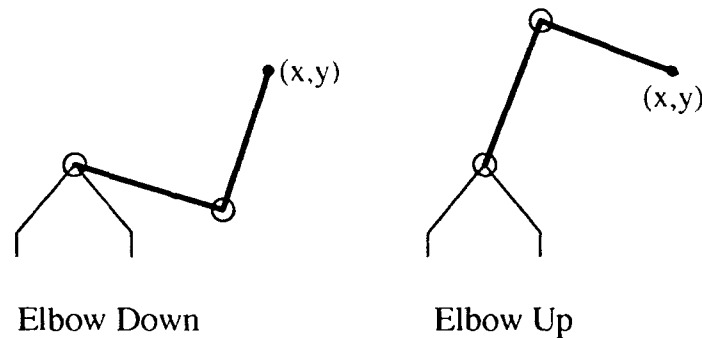


Figure 5.3. "Elbow-Up" and "Elbow-Down" Configurations.

choice, it is still useful to study the efficiency of this configuration to see if any significant differences are present.

Figure 5.4 shows the efficiency using the elbow up solution. Note that the predominant features of the elbow down solution are still present. Efficiency is zero at the workspace edge, and efficiency improves as x -position decreases. However, the general character of the plot has changed noticeably. While the average efficiency in the $x = 0.2\text{ft}$ region was 65-70% for the elbow down configuration, it is only around 45-50% for the elbow up configuration. This is due to the greater moment arm for the second joint in this case. Figure 5.5 shows the torque-speed variation of each actuator during the lifting task executed at $x = 0.2\text{ft}, y = 0.1 \rightarrow 0.8$. Since the moment arm is constant for the first joint, the torque for the first actuator is understandably constant. However, for the "elbow up" configuration, the speed of the first actuator varies significantly, taking it from normal operation in quadrant I through the plugging region and into the regeneration region. This is one cause of the large variations in efficiency seen in Figure 5.4. The second joint does have a varying torque and it is different for each case. Comparing figures 5.2 and 5.4, one can see that even when the elbow up configuration has the first joint in a regenerative mode, at $y \approx 0.8$, the elbow down configuration still provides a better overall efficiency.

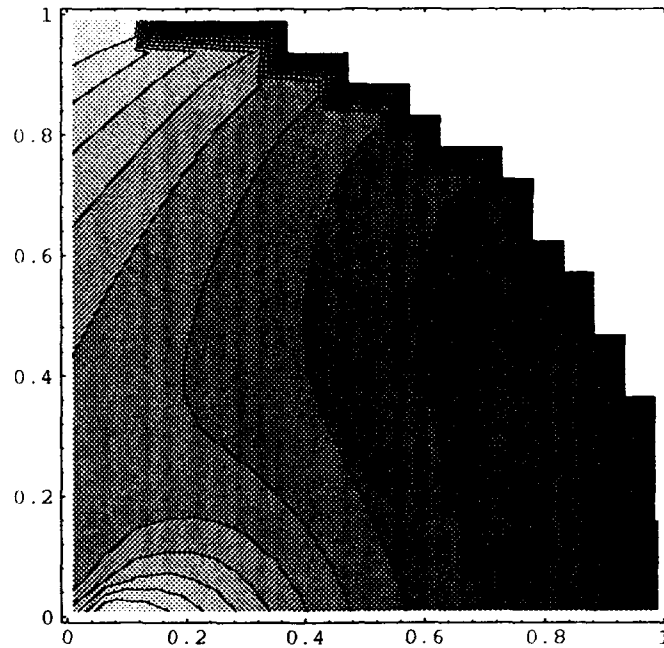


Figure 5.4. Lift Task Efficiency for Two-Link Serial Arm w/ DC Motors ("Elbow Up"). The lightest region represents $\eta_K \geq 91\%$ and the black region represents $\eta_K \leq 9\%$.

Given this comparison, one can conclude that for this robot and task, the job should be done close to the shoulder with the elbow down. This is not a remarkable discovery, as it is already intuitively obvious. This is generally the way a person would lift a heavy load with their arm. However, the analysis can readily be applied to a more complex robot or task.

5.2 Actuator Selection

In the previous example, the actuator type was arbitrarily chosen to be a DC motor. In reality, this choice requires careful consideration, since it can have a dramatic effect on the efficiency of the robot. In this section, hydraulic and electric actuators will be compared using the same two-link serial robot and an assortment of simple tasks. As in the previous section, the task screws are given by equations

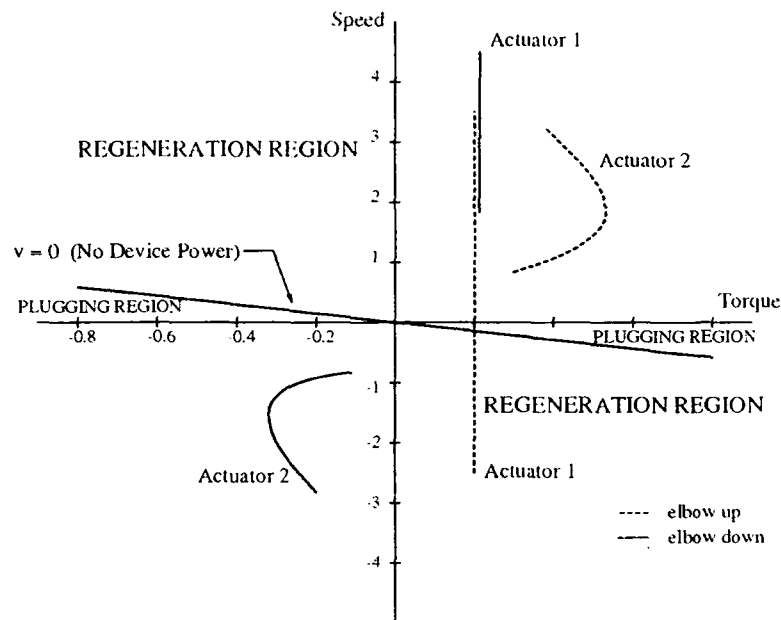


Figure 5.5. Lift Task in Joint Space for Two-Link Serial Arm.

5.1 and 5.2 and the manipulator Jacobian is as shown in equation 5.4. The efficiency measure will vary with the task being compared, and so the device input power will be given by either equation 4.12 or 4.19. For a fair comparison, the constants in these equations will be normalized to eliminate differences in magnitude. This is necessary since no data was available for typical actuators of comparable size.²

To nondimensionalize the DC motor, the method given in (16) was used, in which the fundamental units are based on the rated full load condition of the motor. One unit of angular rotation is equal to the rated full load speed, one unit of torque is equal to the rated torque, one unit of current is equal to the rated current at full load, and other units are derived from these units. Under this convention, the constants k_E and k_T become unity. Then the only constant left to choose is the resistance, R . Typically, DC servomotors have negative slopes of the order of 1 on the torque-speed plot, because this provides good controllability. For example, the

²In general, DC motors have less torque capability than hydraulics.

motor used as a model in the previous section has a slope of -4.65 . From equation 3.21, the slope is seen to be $-R/(k_E k_T)$, so using a slope of -1 , R can be found by solving for R in terms of k_E and k_T :

$$\begin{aligned} -1 &= -\frac{R}{k_E k_T} \\ R &= k_E k_T \end{aligned} \quad (5.5)$$

Then since $k_E = k_T = 1$, $R = 1$ and the device power equation becomes

$$DP = \mathbf{f}^T J J^T \mathbf{f} + \mathbf{f}^T \mathbf{v} \quad (5.6)$$

For the hydraulic case, the equation is nondimensionalized by dividing by the operating pressure, P_S , and the motor constant D_ω . This is equivalent to letting a unit torque equal the peak torque and a unit speed equal the motor constant. Then the device input power equation is

$$DP = \mathbf{n}^T |J^{-1} \mathbf{v}| \quad (5.7)$$

Five tasks were chosen to illustrate the differences in the actuator types. They are:

Lift Task As before, moving an end load vertically in a gravity field. This is a kinetic task with $\mathbf{f} = \{0, 1\}$, $\mathbf{v} = \{0, 1\}$.

Hold Task Holding an end load stationary in a gravity field. This is a reactive task with $\mathbf{f} = \{0, 1\}$, $\mathbf{v} = \{0, 0\}$.

Slow Transport Task Moving the end load slowly along a horizontal path in a gravity field. This is similar to the Hold Task, and is also reactive, with $\mathbf{f} = \{0, 1\}$, $\mathbf{v} = \{0.1, 0\}$.

Fast Transport Task Moving the end load quickly along a horizontal path. In this task, the motion is the primary output, so it is a manipulative task, with $\mathbf{f} = \{0, 0.1\}$, $\mathbf{v} = \{1, 0\}$.

Kinetic Transport Task Moving the load up along a line of slope one. This is a combination of the lift and transport tasks, with $\mathbf{f} = \{0, 1\}$, $\mathbf{v} = \{\frac{\sqrt{2}}{2}, \frac{\sqrt{2}}{2}\}$.

In all the examples of this section, the elbow down configuration was used.

Figures 5.6 and 5.7 show the lift task efficiencies for the DC motor and the hydraulic motor cases, respectively. The DC motor driven robot is essentially the

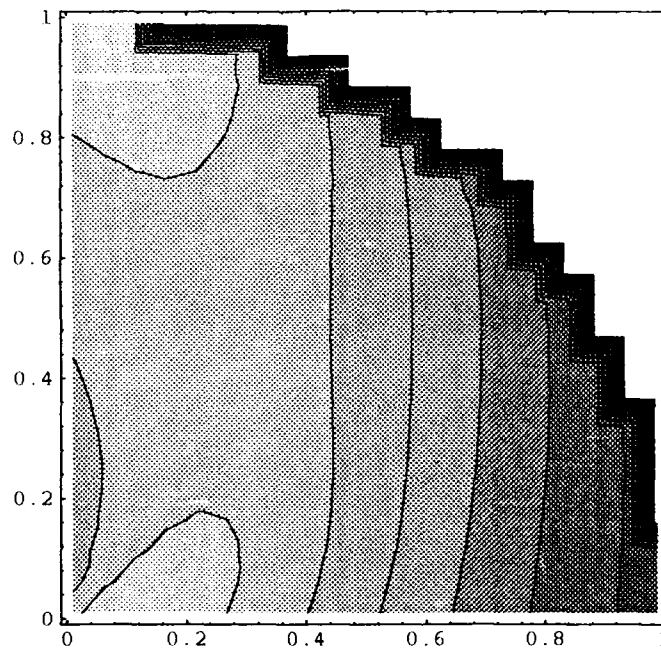


Figure 5.6. Lift Task Efficiency for Two-Link w/DC Motors. The lightest region represents $\eta_K \geq 91\%$ and the black region represents $\eta_K \leq 9\%$.

same as was shown in the previous section, with the highest efficiency occurring near the shoulder. The differences between Figures 5.2 and 5.6 are a result of the change to normalized motor constants. The efficiency plot for the hydraulic case is significantly different than for the electric case. The highest efficiency occurs when the

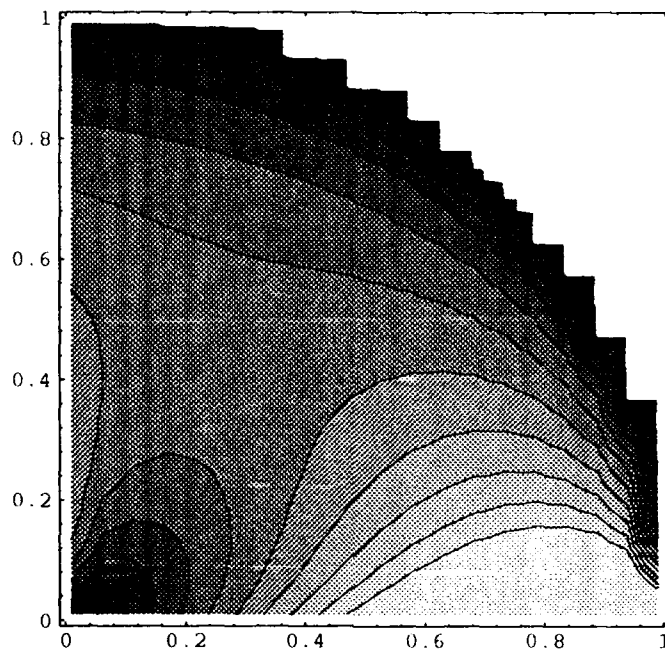


Figure 5.7. Lift Task Efficiency for Two-Link w/Hydraulic Motors. The lightest region represents $\eta_K \approx 50\%$ and the black region represents $\eta_K \leq 9\%$.

arm is stretched out horizontally. This is predictable since the device power depends only on joint velocity, and for low joint velocities given a fixed lift rate, the horizontal distance from the joint to the load should be maximized. The greater torques resulting from this solution do not affect the actuator's efficiency. Another difference not readily seen from the contour plots is that the overall average efficiency is much lower for the hydraulic case. The lightest region of the DC motor plot represents $\eta_K \approx 95\%$, while on the hydraulic plot, it represents $\eta_K \approx 50\%$. The low hydraulic efficiency is the result of two things. First, an individual hydraulic motor can only run at 100% efficiency when the load pressure equals the operating pressure. This condition also equals the maximum torque possible for the motor, so the motor is

rarely operating near 100% efficiency.³ Second, whenever the actuator is providing torque and speed with opposite signs, it continues to draw power, rather than generate power. Compared to the DC motor case, one could say that the hydraulic motor is always "plugging," and cannot regenerate. Whenever the actuators are working against each other, this causes lost "geometric" power and reduces efficiency. This condition is not the dominant cause of inefficiency, however, because the actuators are only operating in quadrant IV of the torque speed plot for a small portion of workspace.

Now consider the hold task. This is a reactive task, so the reactive efficiency measure η_R is used. Figure 5.8 shows the performance of the DC motor. The appearance of the plot is quite similar to figures 5.2 and 5.6. The only difference between the hold task and the lift task is in the velocity required of the actuators. Therefore, this similarity is expected, since the efficiency of a DC motor is primarily dependent on its torque requirement, not on the velocity requirement. No plot is shown for the hydraulic case, since the efficiency is infinite throughout its entire workspace. This is seen from the efficiency equation,

$$\eta_R = \frac{\|\mathbf{f}\|}{\mathbf{n} |J^{-1}\mathbf{v}|} = \frac{1}{0} = \infty$$

This illustrates an important characteristic of the hydraulic-driven robot --- it requires no power to oppose a force when it is stationary.⁴

The slow transport task provides an example similar to the holding task, but allows one to examine the effect of motion in a reactive task. The efficiency of the DC motor case is given by Figure 5.8, just as for the holding task. The plots are

³Another problem with operating near maximum torque is that the maximum joint speed approaches zero as the torque approaches maximum torque, a property seen by referring to the torque-speed plot in Figure 3.6.

⁴This is only true for the ideal hydraulic actuator. Any practical hydraulic actuator would require a small amount of power to counteract leakage in the system. Nevertheless, the power required to hold a load is much lower for a hydraulic system than for an electric system.

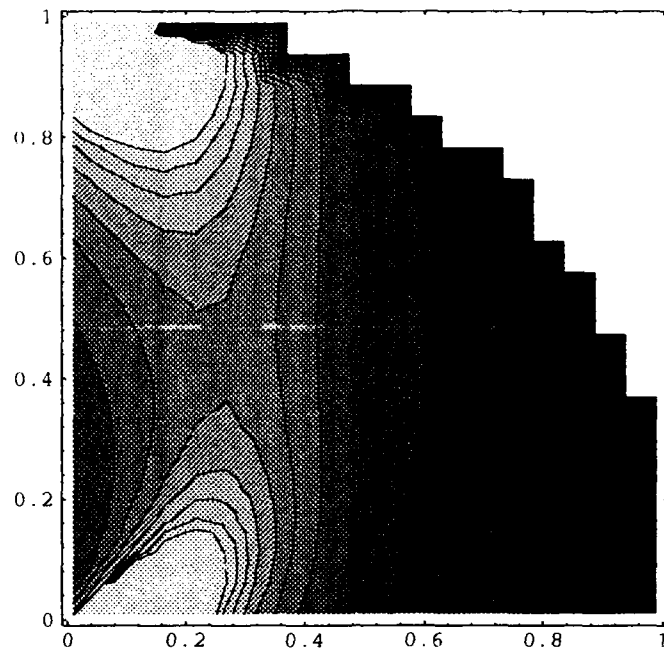


Figure 5.8. Hold Task & Slow Transport Task Efficiency for Two-Link w/DC Motors. The lightest region represents $\eta_R \approx 6$ and the black region represents $\eta_R \approx 0$.

identical because the $\mathbf{f}^T \mathbf{v}$ term in the device power equation is still zero because even force and motion are orthogonal. The efficiency for the hydraulic case is shown in Figure 5.9. The best performance is obtained by positioning the end-effector near the top of the workspace, where joint velocities are the lowest for the horizontal motion. The approximate range of values on this plot is 0 to 8, including a large region of workspace ≥ 5 . Since this performance is only equaled in a small area of the workspace for the electric case, it is evident that the hydraulic actuator driven robot is generally more efficient in completing tasks of this variety.

The fast transport task is essentially the same as the slow transport task, except the emphasis has moved from force to motion. It represents manipulating a light load at high speeds. An example of this type of task is arc welding, where the only load is the weight of the welding rod, which is moved quickly from point to point above a

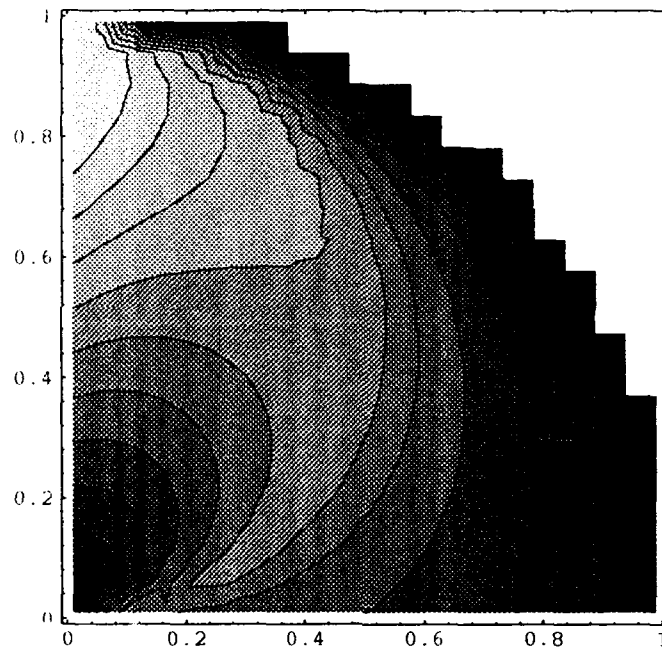


Figure 5.9. Slow Transport Task Efficiency for Two-Link w/Hydraulic Motors. The lightest region represents $\eta_R \approx 8$ and the black region represents $\eta_R \approx 0$.

surface. This is in the category of manipulative tasks, so the metric η_M was used to judge performance. Figures 5.10 and 5.11 show η_M over the workspace of the robot for the electrically and hydraulically driven cases, respectively. Topographically, these plots are identical to those found for the slow transport task. However, the performance index η_M ranges from 0 to 650 for the DC motor and between 0 and 0.9 for the hydraulic motor. Almost all of the workspace for the electric robot provides higher performance in this task than the hydraulic robot.

The final example, kinetic transport, is a combination of lift and transport, with $\|\mathbf{f}\| = \|\mathbf{v}\|$. This is a kinetic task, so the kinetic efficiency metric was used. The efficiency of the DC motor case varies from 0% to 97% in a familiar pattern, shown in Figure 5.12. The efficiency is almost the same as for the lifting case, with only minor variations in the distribution. The torque requirements for each joint are the same as for the lift task, so the similarity is not surprising. However, the

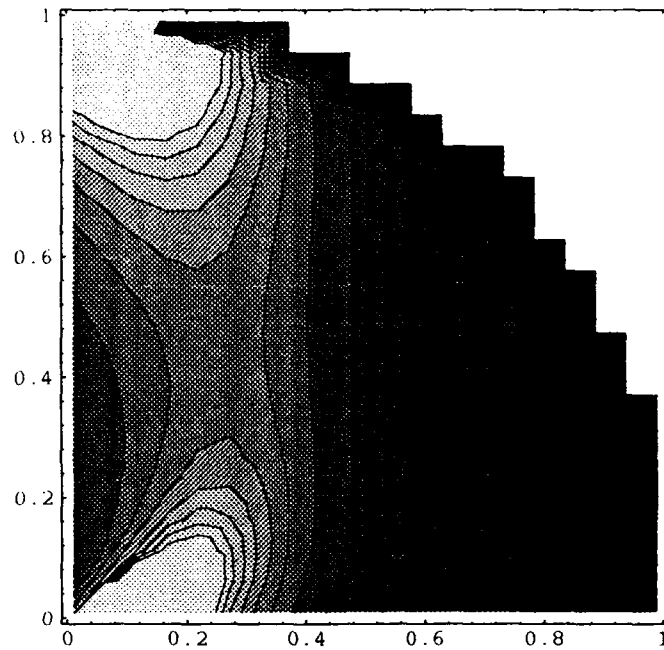


Figure 5.10. Fast Transport Task Efficiency for Two-Link w/DC Motors. The lightest region represents $\eta_M \approx 650$ and the black region represents $\eta_M \approx 0$.

hydraulic efficiency, which is much more sensitive to changes in the velocity portion of the task, presents a quite different pattern than the one seen for the lift task (see Figure 5.13). Rather, the plot is seen to be a blend of the lift and transport tasks (compare this plot with figures 5.7 and 5.9). The efficiency ranges from 0% to 40% with the optimum region occurring above the shoulder at about two-thirds of the maximum reach. Overall, the electric-driven arm appears to provide better power efficiency for this task.

One would need much more specific information about the range of task requirements to decisively determine which actuator type is the best choice, but some general guidelines are clear from this analysis. First, over the majority of the workspace, DC motor driven manipulators are more efficient for kinetic and manipulative tasks, while hydraulics are more efficient for reactive tasks. The welding task mentioned earlier would probably be most efficiently done with DC servomo-

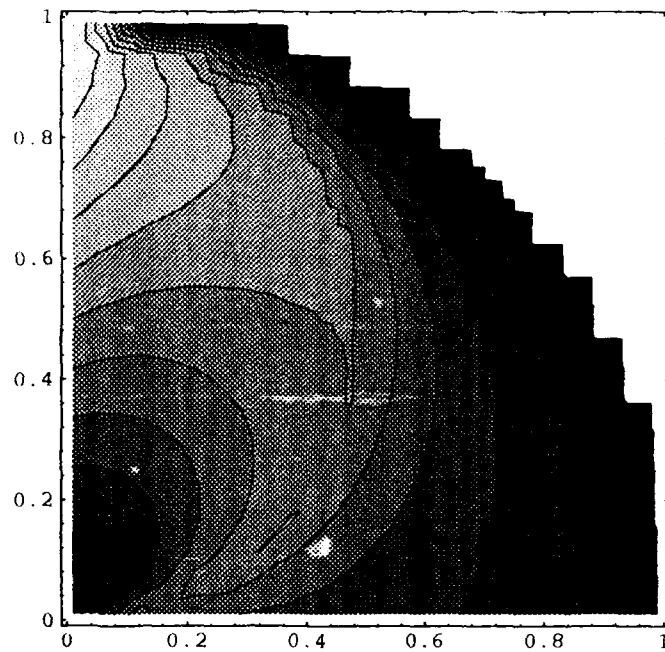


Figure 5.11. Fast Transport Task Efficiency for Two-Link w/Hydraulic Motors. The lightest region represents $\eta_R \approx 0.9$ and the black region represents $\eta_M \approx 0$.

tors, while slowly moving a heavy load is probably best done by hydraulic motors. Second, the optimal performance regions are quite different for hydraulic and electric actuators. This could be an important option for a designer if the entire workspace is not available. For example, for a lift task, if the work area was cramped, the elbow of the arm could get in the way when the end-effector was close to the shoulder. Then the hydraulic actuators might be appropriate, since it performs best without bending the arm at the elbow. One could easily provide a similar scenario in which DC motors would be better.

5.3 Manipulator Structure Selection

In addition to aiding in the selection of an actuator, power analysis can also be used in determining the appropriate kinematic structure to use for a given task.

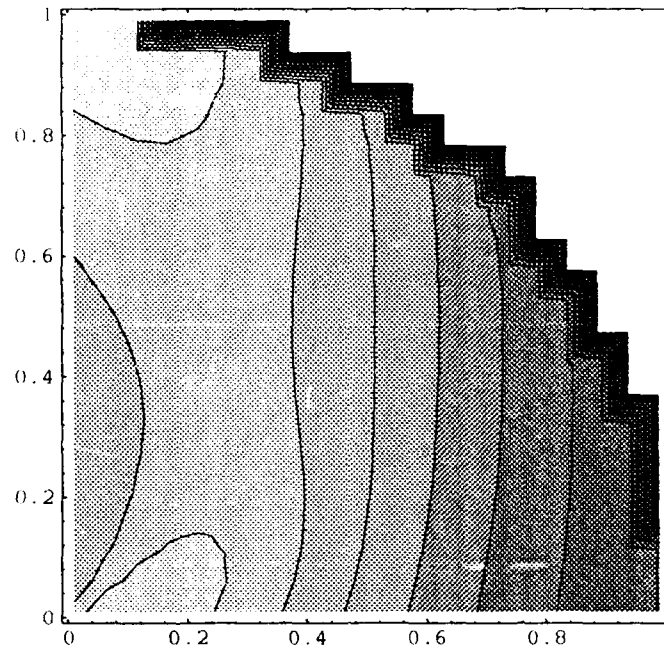


Figure 5.12. Kinetic Transport Task Efficiency for Two-Link w/DC Motors. The lightest region represents $\eta_K \approx 95\%$ and the black region represents $\eta_K \leq 9\%$.

This section will compare a massless parallel type manipulator to the massless serial manipulator used in the previous sections, and the effect of varying link lengths in the serial arm will also be briefly explored.

A 2-DOF parallel arm is shown in Figure 5.14. Both motors are at the base of the manipulator, and independently control the joint angles θ_1 and θ_2' . The end-effector position is described in the same way as for the serial arm, by angles θ_1, θ_2 and lengths a_1, a_2 . From the geometry it is evident that

$$\theta_2' = \theta_1 + \theta_2 \quad (5.8)$$

Differentiating this relation, the equation becomes

$$\dot{\theta}_2' = \dot{\theta}_1 + \dot{\theta}_2 \quad (5.9)$$

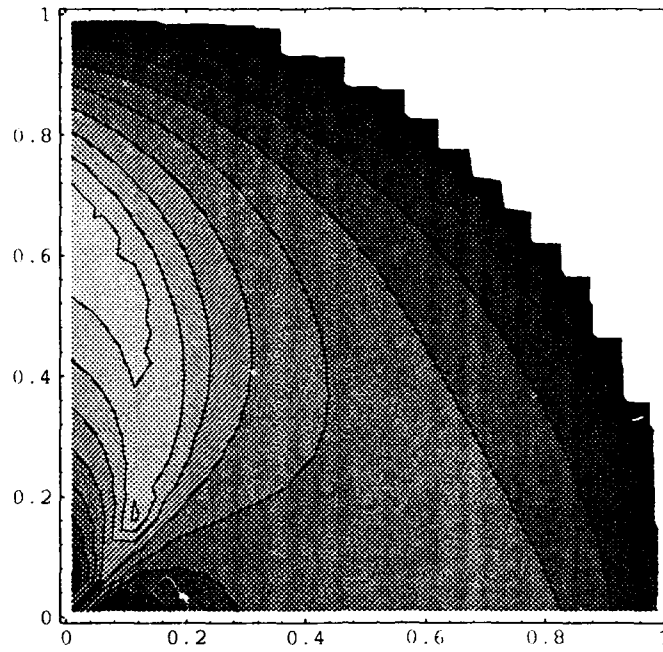


Figure 5.13. Kinetic Transport Task Efficiency for Two-Link w/Hydraulic Motors. The lightest region represents $\eta_K \approx 40\%$ and the black region represents $\eta_K \leq 5\%$.

This relation can be used to derive the parallel Jacobian from the serial Jacobian:

$$J_p = \begin{bmatrix} -s_1 & -s_{12} \\ c_1 & c_{12} \end{bmatrix} \quad (5.10)$$

This Jacobian relates the end-effector velocity to the joint velocities at the motors, $\dot{\theta}_1, \dot{\theta}_2$, but is shown in terms of θ_1, θ_2 . The inverse kinematic equations used to find θ_1, θ_2 are then identical to the ones used for the serial arm's "elbow down" configuration. Using the normalized equations for a DC motor actuated robot, the device power for a parallel arm is given by

$$DP = \mathbf{f}^T J_p J_p^T \mathbf{f} + \mathbf{f}^T \mathbf{v} \quad (5.11)$$

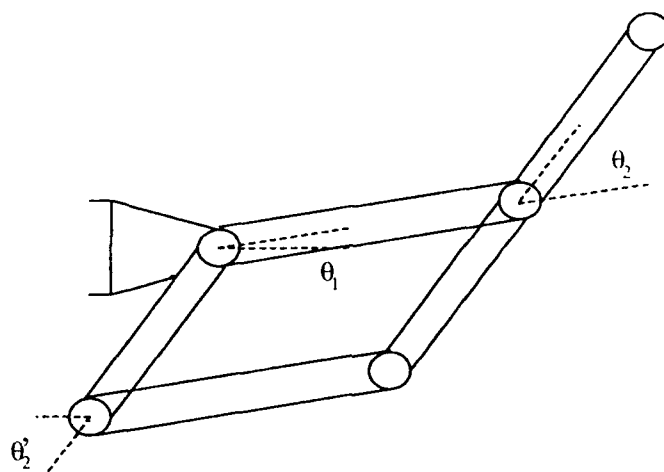


Figure 5.14. Parallel Type 2-DOF Manipulator.

which is identical to equation 4.12 except that J_p is substituted for J .

Now to judge the efficiency of the parallel arm, consider its performance of two tasks that have been previously shown for the serial arm, the lift task and the fast transport task. Figure 5.15 shows the kinetic efficiency (η_K) of the parallel manipulator in the first quadrant workspace. The efficiency varies from 50% to 100%, although the plot still shows the drop to 0%, which is the set value given to areas outside the reachable workspace. Compared to Figure 5.6, it is apparent that the parallel arm is more efficient than the serial arm over a wide range of workspace, although in the vertical band near $x = 0.2$, the serial arm can compete. For the fast transport task, the parallel arm's performance is shown in Figure 5.16. This is a plot of manipulative efficiency (η_M), and again the parallel arm has better overall performance compared to the serial arm, which is shown in Figure 5.10. Similar results were shown by Spenny and Leahy (4), so this is not surprising, but this is another example of the diversity of problems to which power analysis can be applied.

The ratio of the lengths of each link can be changed, providing another option in the structural design of a 2-DOF arm. The usefulness of such a variation to the serial arm can be checked by two possible configurations: 1) let the first link be twice

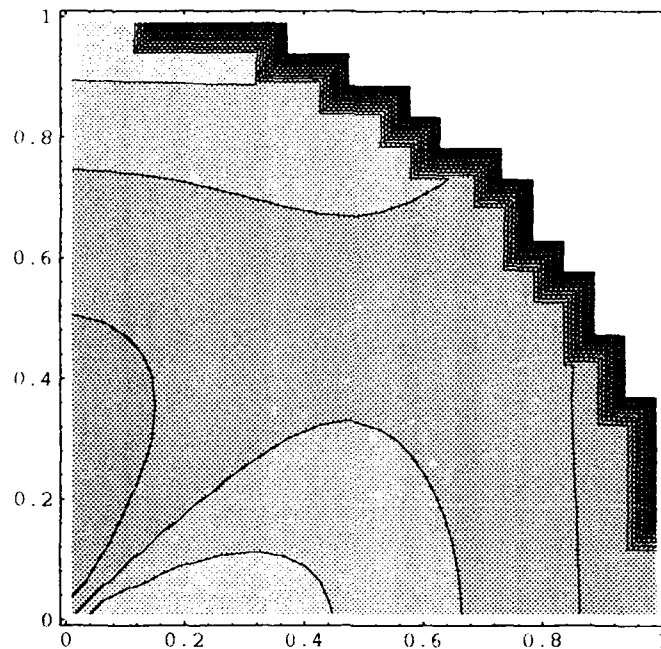


Figure 5.15. Lift Task Efficiency for 2-DOF Parallel Arm w/DC Motors. The lightest region represents $\eta_K \approx 95\%$ and the black region represents $\eta_K \approx 0\%$.

as long as the second, and 2) let the first link be half as long as the second. Figure 5.17 shows the kinetic efficiency of the first case when doing a lift task. Figure 5.18 shows the same task for the second configuration. When compared with Figure 5.6, one can see that the efficiency is similar to the standard two-link arm, with performance falling off as x increases. For the first configuration, however, the drop off is not as fast as for the standard two-link, resulting in an increased overall efficiency. If the reduced reachable workspace was not an issue, this might be a possible method for increasing the power efficiency when performing a lift task.

5.4 Kinematic Redundancy

When a mechanism has more degrees of freedom than its task requires, it is said to be redundant. For kinematic redundancy, this means that the mechanism

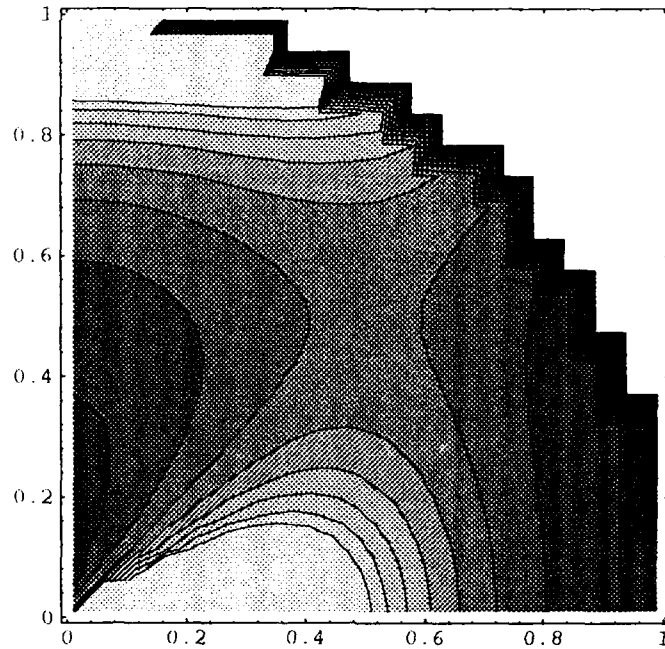


Figure 5.16. Fast Transport Task Efficiency for 2-DOF Parallel Arm w/DC Motors. The lightest region represents $\eta_K \approx 95\%$ and the black region represents $\eta_K \approx 0\%$.

has an infinite choice of joint positions that can complete the task. This choice of joint positions and joint velocities allows the robot to either do more than one task simultaneously, or to do its task while optimizing or maintaining some other condition. Redundancy has been used for singularity avoidance, obstacle avoidance, and the completion of multiple tasks by Nakamura (8) and others.

To illustrate how power analysis can be applied to the choice of redundant solutions, consider a lift task with a three-link serial arm. Let each link length be one, and the task be $\mathbf{f} = \{0, 1\}$, $\mathbf{v} = \{0, 1\}$ starting at a position $(x, y) = (1, 0.25)$. Consider two possible configurations for the manipulator, as shown in Figure 5.19. Which configuration provides the most efficient use of power while completing the

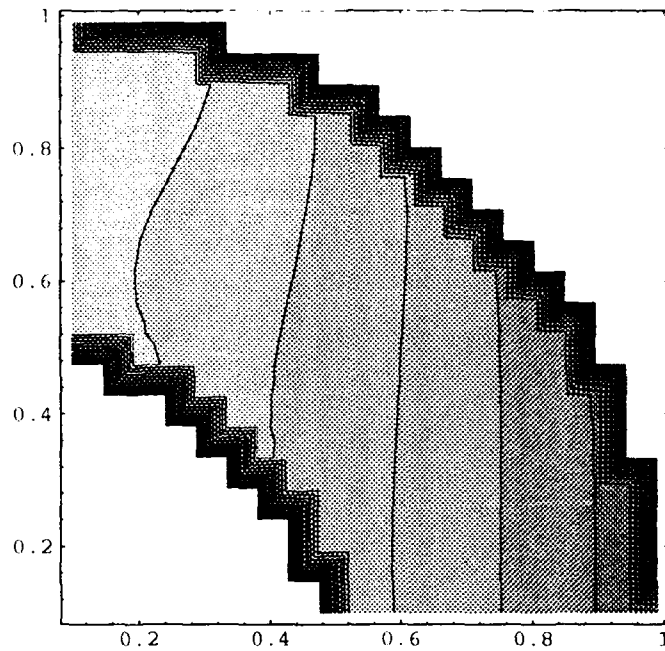


Figure 5.17. Lift Task Efficiency for Two-Link Arm w/DC Motors and $\frac{a_1}{a_2} = 2$. The lightest region represents $\eta_K \approx 95\%$ and the black region represents $\eta_K \approx 0\%$.

task? Recall that kinetic efficiency is given by equation 4.22

$$\eta_K = \frac{\mathbf{w} \circ \mathbf{t}}{DP}$$

Using DC motors at the joints, device power is

$$DP = \mathbf{f}^T J J^T \mathbf{f} + \mathbf{f}^T \mathbf{v} \quad (5.12)$$

so that the efficiency becomes

$$\eta_K = \frac{\mathbf{f}^T \mathbf{v}}{\mathbf{f}^T J J^T \mathbf{f} + \mathbf{f}^T \mathbf{v}} \quad (5.13)$$

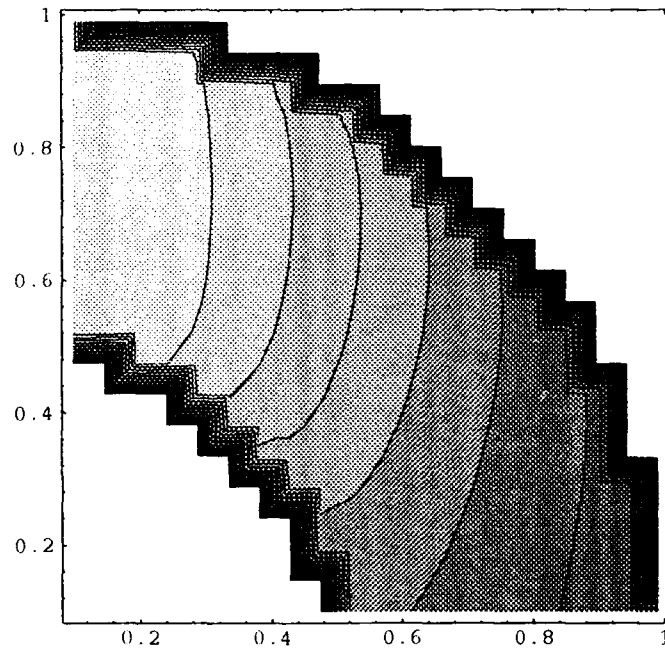


Figure 5.18. Lift Task Efficiency for Two-Link Arm w/DC Motors and $\frac{a_1}{a_2} = \frac{1}{2}$. The lightest region represents $\eta_K \approx 95\%$ and the black region represents $\eta_K \approx 0\%$.

in which \mathbf{f}, \mathbf{v} have been defined above and the Jacobian is

$$J(\boldsymbol{\theta}) = \begin{bmatrix} -s_1 - s_{12} - s_{123} & -s_{12} - s_{123} & -s_{123} \\ c_1 + c_{12} + c_{123} & c_{12} + c_{123} & c_{123} \end{bmatrix} \quad (5.14)$$

For the first configuration, shown in gray in the figure, $\boldsymbol{\theta}_1 = (2.87, -2.69, -0.38)^T$ and the device power is 6.8, for an efficiency of $\eta_{K1} = 14.6\%$. The second configuration, shown in black, has angles $\boldsymbol{\theta}_2 = (1.71, -1.46, -1.65)^T$, which leads to a device input power of 3.33, and an efficiency of $\eta_{K2} = 30.1\%$. Clearly, the selection of the configuration can greatly affect the efficiency of the robot in performing the task.

If the task and robot are fixed, then one can easily find the optimum configuration for the manipulator by minimizing $DP(\boldsymbol{\theta})$, using any standard optimization technique. A more interesting problem, however, is when a robot must perform many

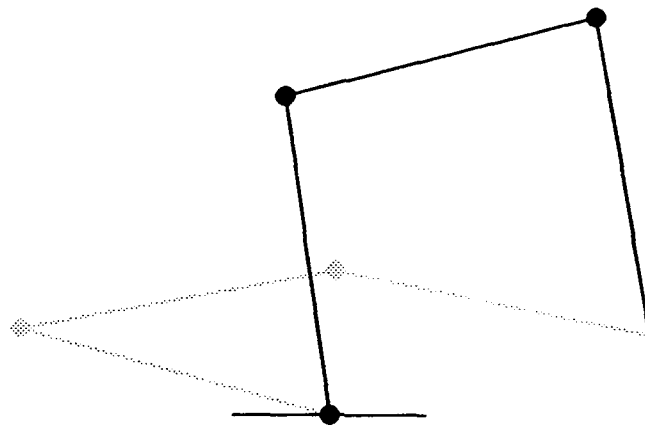


Figure 5.19. Two Possible Joint Configurations for Three-Link Serial Arm.

different tasks in a sequential fashion, and cannot always be configured in advance for each one. Then it would be useful if the robot could be controlled in such a way that it “seeks out” the most efficient configuration, while simultaneously performing the task.

One solution to this problem can be derived using Nakamura’s task priority equations (8:pp.126-131), coupled with the device input power as a potential function. Suppose the given task is constant, and let the starting configuration be arbitrary, as if the robot had just finished a different task. The object is to complete the task while altering the configuration to improve efficiency. The joint velocities can be commanded by using the equation for a kinematically redundant mechanism, equation 4.8

$$\dot{\theta} = J^{\#} \mathbf{v} + (I - J^{\#} J) \mathbf{z}$$

but let the arbitrary vector \mathbf{z} be defined by

$$\mathbf{z} = -k \left(\frac{\partial DP}{\partial \boldsymbol{\theta}} \right)^T \quad (5.15)$$

Then the commanded joint velocities are

$$\dot{\boldsymbol{\theta}} = J^\# \mathbf{v} - (I - J^\# J) k \left(\frac{\partial DP}{\partial \boldsymbol{\theta}} \right)^T \quad (5.16)$$

This choice of joint velocities will result in the proper motion of the end-effector (\mathbf{v}), but will also work to reconfigure the manipulator so as to minimize device power DP . This in turn optimizes η_K , since the output power is constant. Suppose the task requires no motion, so that $\mathbf{v} = 0$. Then

$$\begin{aligned} \frac{d}{dt}(DP) &= \left(\frac{\partial DP}{\partial \boldsymbol{\theta}} \right) \dot{\boldsymbol{\theta}} \\ &= \frac{\partial DP}{\partial \boldsymbol{\theta}} \left[-(I - J^\# J) k \left(\frac{\partial DP}{\partial \boldsymbol{\theta}} \right)^T \right] \\ &= -k \left(\frac{\partial DP}{\partial \boldsymbol{\theta}} \right) (I - J^\# J) (I - J^\# J)^T \left(\frac{\partial DP}{\partial \boldsymbol{\theta}} \right)^T \\ &\leq 0 \end{aligned}$$

when $k > 0$. This uses the idempotency and symmetry of $(I - J^\# J)$. Since k is chosen in the design of the control law, then device power can be designed to have a monotonic decline for a stationary task. This does not guarantee $\frac{d}{dt}(DP) \leq 0$ for $\mathbf{v} \neq 0$, but the second term always will operate to reduce DP as much as possible while still completing the task.

This scheme was applied to the lifting task through the use of a *Mathematica* routine (Appendix A) to show the increase in efficiency during the performance of the task. The starting position was taken as the less efficient (gray) configuration in Figure 5.19 and the arm was allowed to run for 5 seconds. The task has been

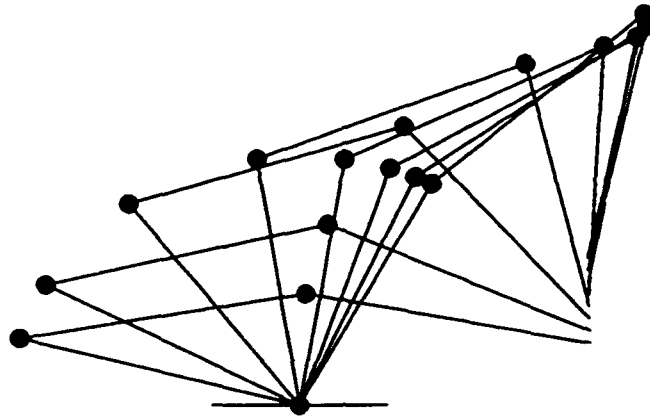


Figure 5.20. Motion of Kinematically Redundant Arm Performing a Lift Task While Optimizing Efficiency.

modified slightly to $\mathbf{f} = \{0, 0.1\}$, $\mathbf{v} = \{0, 0.1\}$ which does not change efficiency in any way, but allows a longer time to elapse for a small total lift distance. The motion of the arm is shown in Figure 5.20. Note how the robot end-effector moves straight up, as required by the task, but the configuration changes to approach the most efficient position for the task. It actually passes through the black configuration of Figure 5.19, indicating that this was not the optimum configuration. The efficiency increase of the mechanism is shown by Figure 5.21, which shows the efficiency over time. In contrast, if the device power is not used to drive the robot to increased efficiency, but rather only the first term of equation 4.8 is used, then the robot moves as shown in Figure 5.22. The task is still performed, but the shape of the arm remains relatively unchanged, since this solution provides as little joint speed as possible.⁵ The difference in the two solutions can be substantial in terms of the

⁵This solution is the $\dot{\theta}$ that has the minimum norm $||\dot{\theta}||$.

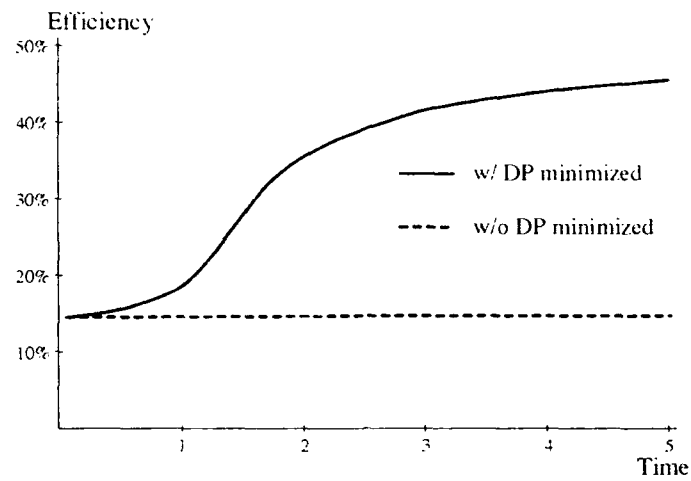


Figure 5.21. Efficiency of Serial Three-Link During a Lift Task.

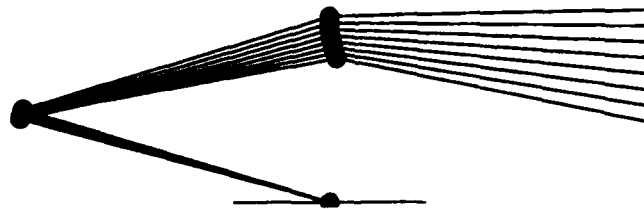


Figure 5.22. Motion of Kinematically Redundant Arm Performing a Lift Task While NOT Optimizing Efficiency.

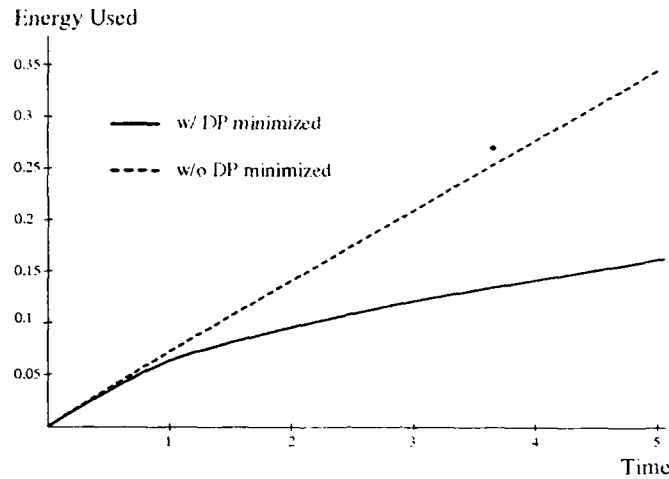


Figure 5.23. Energy Use of Serial Three-Link During a Lift Task. Energy is defined as $E(t) = \int_0^t DP(\tau) d\tau$

energy used to complete the task, as shown in Figure 5.23. About twice as much energy is used when the redundancy is not utilized.

The choice of the constant k in this control scheme was said to be arbitrary, subject only to the constraint $k > 0$. In the above simulation, k was set to one. Increasing k results in a faster response, moving the manipulator to the optimum location very quickly. However, in the end, k must be chosen based on the maximum possible joint speed, so that the control will not saturate the motors.

While this method does work to improve efficiency, it is not without problems as a control scheme. The foremost problem is that the method does not avoid singularity points of the manipulator. At these points, the joint velocities required for an arbitrary motion can be very large, which is generally seen by the "blowing up" of the Jacobian inverse or pseudoinverse. Unfortunately, the singularity was artificially removed from the device power equation when J^{-1} was cancelled by a J ($\tau^T \dot{\theta} = \mathbf{f}^T J J^{-1} \mathbf{v} = \mathbf{f}^T \mathbf{v}$). The result is that no penalty is assessed for these infinite velocities, because the corresponding torque is near zero. If the DC motor was more precisely modelled, terms would be introduced that would force device power to

infinity when infinite speeds were required. For example, if motor windage losses were added, it would have a term of the form $\mathbf{v}^T (J^{-1})^T J^{-1} \mathbf{v}$ in the device power equation, which would go to infinity at singular points. Another possible solution is to add $k_2 J^{-1}(\boldsymbol{\theta})$ to $DP(\boldsymbol{\theta})$ to create a new potential function. Then, using the values of k and k_2 , the control law could weight the importance of avoiding singular points against the importance of improved efficiency.

In light of this last concern, it is also interesting to reconsider the problem, substituting hydraulic motors for the DC motors at the joints. Then the device power is given by

$$DP = \mathbf{n}^T [J^\# \mathbf{v} + (I - J^\# J) \mathbf{z}] \quad (5.17)$$

and equation 5.13 becomes

$$\eta_K = \frac{\mathbf{f}^T \mathbf{v}}{\mathbf{n}^T [J^\# \mathbf{v} + (I - J^\# J) \mathbf{z}]} \quad (5.18)$$

From this equation, it is apparent that the minimization of the device power for the hydraulic robot will also be effective in avoiding singularities, since $\|J^\# \mathbf{v}\| \rightarrow \infty$, $\eta_K \rightarrow 0$ as singular points are approached. However, a new problem emerges since \mathbf{z} is still in the device power equation for the kinematically redundant hydraulic actuator case, whereas it did not appear in the device power equation for the kinematically redundant DC motor case. Now there are two optimization problems, one in which the best configuration must be chosen, and one in which the best distribution of velocities in the joints must be chosen. A method to solve this is to define a new "state" vector for the system including not only the joint configuration $\boldsymbol{\theta}$, but also the arbitrary vector \mathbf{z} ,

$$\boldsymbol{\phi} = \begin{bmatrix} \boldsymbol{\theta} \\ \mathbf{z} \end{bmatrix} \quad (5.19)$$

Then the device power is a function of ϕ , and equation 5.16 can be written

$$\dot{\phi} = A\mathbf{x} - kB \left(\frac{\partial DP}{\partial \phi} \right)^T \quad (5.20)$$

where

$$A = \begin{bmatrix} J^\# & \mathbf{0} \\ \mathbf{0} & \mathbf{0} \end{bmatrix}$$

$$\mathbf{x} = \begin{bmatrix} \mathbf{v} \\ \mathbf{0} \end{bmatrix}$$

$$B = \begin{bmatrix} I - J^\# J & \mathbf{0} \\ \mathbf{0} & I \end{bmatrix}$$

$$\frac{\partial DP}{\partial \phi} = \begin{bmatrix} \frac{\partial DP}{\partial \theta} & \frac{\partial DP}{\partial \mathbf{z}} \end{bmatrix}$$

Note that B is idempotent and symmetric, so that when $\mathbf{x} = \mathbf{0}$,

$$\begin{aligned} \frac{d}{dt}(DP) &= \frac{\partial DP}{\partial \phi} \dot{\phi} \\ &= -k \frac{\partial DP}{\partial \phi} B \left(\frac{\partial DP}{\partial \phi} \right)^T \\ &= -k \left(\frac{\partial DP}{\partial \phi} \right) B B^T \left(\frac{\partial DP}{\partial \phi} \right)^T \\ &\leq 0 \end{aligned}$$

as before. This method has not been simulated because the actual expression of device power in terms of θ is much more complex than for the electric case, and requires a more sophisticated numerical routine. Unfortunately, the time for the development of such a routine was not available.

5.5 Actuator Redundancy Resolution

The final example of power analysis' usefulness is a simple demonstration of how the distribution of torques in a mechanism can be chosen by picking the combination that provides the most efficient use of power.

Recall that for a mechanism with redundant actuators, driven by nondimensionalized DC motors, the device input power can be written

$$DP = \mathbf{w}^T J_v G S S^{\#} G^T J_v^T \mathbf{w} + \mathbf{y}^T (I - S S^{\#}) \mathbf{y} + \mathbf{w}^T J_v G S S^{\#} (J_v^{-1} T \mathbf{t})_{Act} + \mathbf{y}^T (I - S S^{\#}) (J_v^{-1} T \mathbf{t})_{Act} \quad (5.21)$$

Then to minimize DP with respect to the arbitrary vector \mathbf{y} , the condition

$$\frac{\partial DP}{\partial \mathbf{y}} = \mathbf{0} \quad (5.22)$$

must be met. Using the symmetry of $(I - S S^{\#})$, this partial derivative can be written:

$$\frac{\partial DP}{\partial \mathbf{y}} = 2(I - S S^{\#}) \mathbf{y} + (I - S S^{\#}) (J_v^{-1} T \mathbf{t})_{Act} = \mathbf{0} \quad (5.23)$$

Then combining terms,

$$\frac{\partial DP}{\partial \mathbf{y}} = (I - S S^{\#}) [2\mathbf{y} + (J_v^{-1} T \mathbf{t})_{Act}] = \mathbf{0} \quad (5.24)$$

Now let $\mathbf{x} = 2\mathbf{y} + (J_v^{-1} T \mathbf{t})_{Act}$, and the equation becomes:

$$(I - S S^{\#}) \mathbf{x} = \mathbf{0} \quad (5.25)$$

When redundancy exists, $(I - S S^{\#}) \neq \mathbf{0}$, and the solution is:

$$\mathbf{x} = S S^{\#} \mathbf{q} \quad (5.26)$$

where \mathbf{q} is an arbitrary vector. Then solving for \mathbf{y} in terms of \mathbf{q} ,

$$2\mathbf{y} + (J_v^{-1}T\mathbf{t})_{Act} = SS^\# \mathbf{q} \quad (5.27)$$

$$\mathbf{y} = \frac{1}{2}SS^\# \mathbf{q} - \frac{1}{2}(J_v^{-1}T\mathbf{t})_{Act} \quad (5.28)$$

Then the optimal choice for torque distribution can be found by substituting this back into the torque equation to get

$$\begin{aligned} \tau_a &= SS^\# G^T J_v^T \mathbf{w} + (I - SS^\#) \left[\frac{1}{2}SS^\# \mathbf{q} - \frac{1}{2}(J_v^{-1}T\mathbf{t})_{Act} \right] \\ \tau_a &= SS^\# G^T J_v^T \mathbf{w} - \frac{1}{2}(I - SS^\#)(J_v^{-1}T\mathbf{t})_{Act} \end{aligned} \quad (5.29)$$

Note that the arbitrary vector \mathbf{q} disappears from the torque expression. This value for torque in turn produces a device power of

$$\begin{aligned} DP &= \mathbf{w}^T J_v G S S^\# G^T J_v^T \mathbf{w} + \mathbf{w}^T J_v G S S^\# (J_v^{-1}T\mathbf{t})_{Act} \\ &\quad - \frac{1}{4}(J_v^{-1}T\mathbf{t})_{Act}^T (I - SS^\#)(J_v^{-1}T\mathbf{t})_{Act} \end{aligned} \quad (5.30)$$

Consider a task where a two-link serial arm is required to push against a stationary object as shown in Figure 5.24. As was discussed earlier, when an open loop mechanism comes in contact with the environment it becomes a closed loop mechanism. In this case, only one actuator is required to produce the desired force, and the other actuator is redundant. If the robot is treated as a *non-redundant* mechanism, then the required joint torques are

$$\begin{aligned} \boldsymbol{\tau} &= J^T \mathbf{f} \\ \boldsymbol{\tau} &= \begin{bmatrix} -1.32 \\ 0.48 \end{bmatrix} \end{aligned}$$

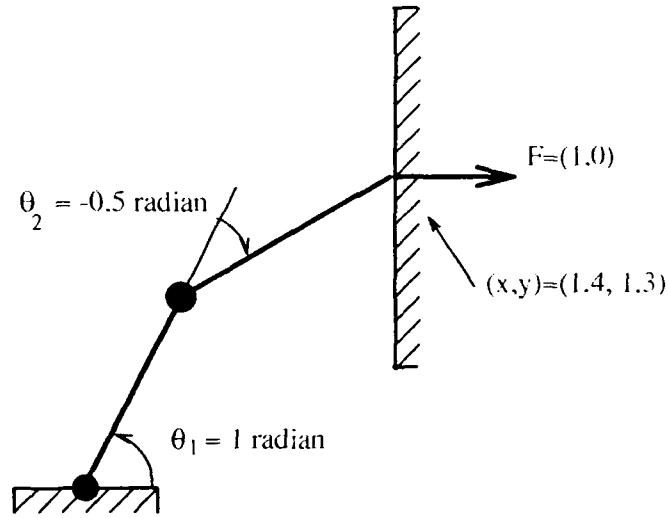


Figure 5.24. Task with Redundant Actuation

for the θ_1 , θ_2 , and \mathbf{f} shown in the figure. Since there is no motion, $\dot{\boldsymbol{\theta}} = (0,0)^T$, and device power is

$$\begin{aligned} DP &= \boldsymbol{\tau}^T \boldsymbol{\tau} + \boldsymbol{\tau}^T \dot{\boldsymbol{\theta}} = \boldsymbol{\tau}^T \boldsymbol{\tau} \\ &= 1.97 \end{aligned} \quad (5.31)$$

Since this is a reactive task, reactive efficiency is used and

$$\eta_R = \frac{\|\mathbf{f}\|}{DP} \approx 0.5 \quad (5.32)$$

Now compare this to the result obtained by using the equation for optimal redundant torque actuation, equation 5.29. In this example, $\mathbf{w} = \mathbf{f}$ and $\mathbf{t} = 0$. The matrix G is given by

$$G = \begin{bmatrix} I \\ \frac{\partial \mathbf{f}}{\partial \boldsymbol{\theta}_2} \\ \frac{\partial \mathbf{f}}{\partial \boldsymbol{\theta}_1} \end{bmatrix} = I \quad (5.33)$$

$G = I$ because no open loop joints are virtually actuated. The matrix S is given by

$$S = \begin{bmatrix} 1 \\ \frac{\partial \theta_2}{\partial \theta_1} \end{bmatrix} = \begin{bmatrix} 1 \\ \frac{\pi c_1}{c_{12}} - 1 \end{bmatrix} = \begin{bmatrix} 1 \\ -1.6 \end{bmatrix} \quad (5.34)$$

and J_v is the standard two-link Jacobian. Then the torque is

$$\tau_a = \begin{bmatrix} 1 \\ -1.6 \end{bmatrix} \begin{bmatrix} 0.277 & -0.447 \end{bmatrix} \begin{bmatrix} 1 & 0 \\ 0 & 1 \end{bmatrix} \begin{bmatrix} -1.32 \\ -0.48 \end{bmatrix} + \begin{bmatrix} 0 \\ 0 \end{bmatrix} \quad (5.35)$$

$$\tau_a = \begin{bmatrix} -0.15 \\ 0.24 \end{bmatrix} \quad (5.36)$$

Note that when $\mathbf{t} = 0$, the optimal choice for \mathbf{y} becomes $\mathbf{y} = \mathbf{0}$. Using this torque vector, the device power becomes

$$DP = \tau_a^T \tau_a = 0.0821 \quad (5.37)$$

and reactive efficiency is

$$\eta_R = \frac{1}{0.0821} \approx 12 \quad (5.38)$$

This demonstrates that with the optimal choice of torque distribution, the performance of the robot in terms of power efficiency is greatly improved.

It can easily be shown by a statics analysis that this torque distribution still exerts a horizontal force on the wall of $f_x = 1$. The difference (other than reduced input power) is that the reaction forces in the vertical direction are changed. The vertical force is zero for the first case, but $f_y = -0.8210$ when the torque is calculated for the optimal efficiency case. The fact that this non-zero vertical force is generated is a possible problem with this method when applied to open-loop systems that become closed-loop systems by contact with the environment. If the method is applied to a real closed-loop mechanism, the change in forces at the point where

the virtual cut is made would be completely internal, and have no effect on the task. However, this does not mean that the method cannot be used as shown in the example, it only means that some other constraint on the torques may exist. In the example, to reach the optimal torque distribution, the coefficient of friction between the wall and the end-effector would have to be greater than 0.824. If $\mu < 0.824$, then the end-effector would slip before this torque distribution was reached. This type of constraint can be expected to surface in applying this method to many areas of robotics, such as optimal grasping, but can still be useful.

VI. Conclusion

The purpose of this thesis was to develop a means of measuring and using the energy efficiency of robotic devices. This required a consistent method of describing the task mathematically, a measurement of the task output, an expression for the power required by the device, and a metric which combined these elements into a scalar quantity that one could use to judge how efficiently the mechanism performed the task.

The function of most mechanisms can be stated by describing the motion of the mechanism and the forces that it exerts on the environment. Often the motion is a complex path, and the forces will change as the device moves from start to finish in the accomplishment of its function. In addition, some mechanisms, such as robots, are multi-functional, creating an even more complex system of tasks to describe. *At any given instant, however*, the motion and exerted force of the device can be considered constant. These quantities can then be written as two screws, the twist and the wrench, and this screw pair is then considered to be the instantaneous task of the mechanism.

For some functions, one of the two defining qualities may be of greater importance than the other. For example, when writing, the motion of the pencil tip is much more crucial than the force exerted by the tip on the paper. The relative importance of the force and motion can be used to divide tasks into three types: kinetic, manipulative, and reactive. In kinetic tasks, force and motion are equally important; in manipulative tasks, motion is most important; and in reactive tasks, force is most important.

Given these task types it is evident that no single metric is appropriate for all tasks. Therefore, we developed a metric for each task type. For kinetic tasks, the performance was judged by the standard efficiency measure of the ratio of output

power to input power. For manipulative tasks, the metric used divides the twist magnitude by the input power, and for reactive tasks, the wrench magnitude was divided by the input power.

The input power was found to be a function of the task, the geometric configuration, and the type of actuator used by the mechanism. When redundancy exists in the mechanism, it was shown that the expression for input power contained an arbitrary term that could be used to change the power requirements for a given task.

After establishing the method for measuring the efficiency in chapter IV, chapter V demonstrated some of the ways in which robotics systems can be designed so as to optimize energy efficiency. It was shown that the location of the task, relative to the robot base, can be chosen to improve efficiency, and that when multiple inverse kinematic solutions exist, they do not necessarily have the same efficiency for a given task. It was also found that DC motor driven robots are generally more efficient than hydraulic actuated robots when performing kinetic and manipulative tasks, but that hydraulics are more efficient for reactive tasks. Power analysis was also shown to be a useful tool in determining the most efficient mechanical structure for a robot. In particular, for many tasks, a parallel-type arm is more efficient than a serial arm.

Redundancy resolution can also be accomplished by power analysis. A method was developed for controlling a serial arm with kinematic redundancy, and numerical simulations demonstrated the ability of the algorithm to decrease energy use in a lifting task. Actuation redundancy can also be used to improve efficiency.

Since this area has not been extensively studied, this paper has tried to lay a mathematical foundation for power analysis, and survey some of the possible applications. Future work is needed to supplement this thesis in many areas. First, experimental evidence is required to verify the basic equations and the actuator models. Second, the applications should be explored in much greater detail. In particular, the analysis of closed chain mechanisms should be expanded, to extend its

application to optimal grasping. Finally, expanded actuator models could be developed, which may allow a more accurate picture of how a mechanisms motion and force affect its power use.

The field of robotics is relatively young, and until recently, most research in robotics has been in developing methods to design and control robots in a variety of tasks. This goal has been nearly reached, as the kinematics and control of manipulators is well understood. I believe that the goal of robotics engineers in the future should be to create robots that not only work, but work efficiently. I hope that this thesis may contribute in some way to the attainment of this goal.

Appendix A. Mathematica *Routine Used For Kinematic Redundancy*

Example

(*This Mathematica file will simulate a three-link serial arm performing a lifting task. *)

(*The equations below are for finding the inverse kinematic solution. They are not used by the Q functions, but are for troubleshooting purposes. *)

j2x:= ex - Cos[tt]

j2y:= ey - Sin[tt]

d:=(j2x^2 + j2y^2 -2)/(2)

t2:=ArcTan[d,-Sqrt[1-d^2]]

t1:=ArcTan[j2x,j2y] - ArcTan[1+ Cos[t2], Sin[t2]]

t3:=tt-t2-t1

px[t1_,t2_,t3_]:= Cos[t1] + Cos[t1+t2] + Cos[t1+t2+t3]

py[t1_,t2_,t3_]:= Sin[t1] + Sin[t1+t2] + Sin[t1+t2+t3]

(* The dpt[] function calculates the partial time derivative of the device power. *)

```

dpt[t1_,t2_,t3_] := {2*(Cos[t1 + t2] + Cos[t1 + t2 + t3])*
  (-Sin[t1 + t2] - Sin[t1 + t2 + t3]) +
  2*(Cos[t1] + Cos[t1 + t2] + Cos[t1 + t2 + t3])*
  (-Sin[t1] - Sin[t1 + t2] - Sin[t1 + t2 + t3]) -
  2*Cos[t1 + t2 + t3]*Sin[t1 + t2 + t3],
2*(Cos[t1 + t2] + Cos[t1 + t2 + t3])*
  (-Sin[t1 + t2] - Sin[t1 + t2 + t3]) +
  2*(Cos[t1] + Cos[t1 + t2] + Cos[t1 + t2 + t3])*
  (-Sin[t1 + t2] - Sin[t1 + t2 + t3]) -
  2*Cos[t1 + t2 + t3]*Sin[t1 + t2 + t3],
-2*Cos[t1 + t2 + t3]*Sin[t1 + t2 + t3] -
  2*(Cos[t1 + t2] + Cos[t1 + t2 + t3])*Sin[t1 + t2 + t3] -
  2*(Cos[t1] + Cos[t1 + t2] + Cos[t1 + t2 + t3])*Sin[t1 + t2 + t3]}

```

(* j[] is the manipulator Jacobian, jp[] is its pseudoinverse. *)

```

j[t1_,t2_,t3_] := {{-Sin[t1] - Sin[t1 + t2] - Sin[t1 + t2 + t3],
  -Sin[t1 + t2] - Sin[t1 + t2 + t3], -Sin[t1 + t2 + t3]},
{Cos[t1] + Cos[t1 + t2] + Cos[t1 + t2 + t3],
  Cos[t1 + t2] + Cos[t1 + t2 + t3], Cos[t1 + t2 + t3]}}

```

```

jp[t1_,t2_,t3_] := pinv[j[t1,t2,t3]]

```

(* dp[] calculates the device power, eff[] calculates efficiency.
*)

```
dp[t1_,t2_,t3_]:= f.v + f.j[t1,t2,t3].T[j[t1,t2,t3]].f
```

```
eff[t1_,t2_,t3_]:= f.v/dp[t1,t2,t3]
```

```
(* The expressions below set the intial variables for the task. *)
```

```
f:={0,.1}
```

```
v:={0,.1}
```

```
k:=1
```

```
x0:=0
```

```
xf:= .3
```

```
dx:=.1
```

```
q0:=0
```

```
q=q0
```

```
t0:={2.87071,-2.68862,-.382089}
```

```
t=t0
```

```
dt0:={0,0,0}
```

```
dt=dt0
```

```
tv=Table[0,{z,51}]
```

```
qv=Table[0,{z,51}]
```

```
effv=Table[0,{z,51}]
```

```
dpv=Table[0,{z,51}]
```

```
(*The function Q[w_] runs a simulation of the lift task from t=0 to  
t=w, using the kinematically redundant equations. The Q0[w_]   
function runs the same simulation without taking advantage of  
redundancy. *)
```

```

Q[w_]:= Block[{t=t0,dt=dt0,q=0}, Do[t=N[t+dt dx]; a=N[t[[1]]];
b=N[t[[2]]]; c=N[t[[3]]]; dt = N[jp[a,b,c].v - k (Id[3]
-jp[a,b,c].j[a,b,c]).dpt[a,b,c]]; q = N[q + N[dp[a,b,c] dx]];
i=Floor[10.01 x + 1]; tv[[i]] = t; effv[[i]] = N[eff[a,b,c]];
dpv[[i]] = N[dp[a,b,c]];qv[[i]]=q, {x,x0,w,dx}];Print[q]]

```

```

Q0[w_]:= Block[{t=t0,dt=dt0,q=0}, Do[t=N[t+dt dx]; a=N[t[[1]]];
b=N[t[[2]]]; c=N[t[[3]]]; dt = N[jp[a,b,c].v]; q = N[q +
N[dp[a,b,c] dx]]; i=Floor[10.01 x + 1]; tv[[i]] = t; effv[[i]] =
N[eff[a,b,c]]; dpv[[i]] = N[dp[a,b,c]];qv[[i]]=q,
{x,x0,w,dx}];Print[q]]

```

(*The functions below draw a picture of the motion simulated by Q[] or Q0[], using Mathematica's graphics primitives. *)

```

G[t1_,t2_,t3_,g_]:=Graphics[{GrayLevel[g],Line[{{0,0},{x1[t1],y1
[t1]},{x2[t1,t2],y2[t1,t2]},{x3[t1,t2,t3],y3[t1,t2,t3]}}],Line[{{-
.3,0},{.3,0}}],PointSize[0.03],Point[{0,0}],Point[{x1[t1],y1[t1]}]
,Point[{x2[t1,t2],y2[t1,t2]}]}]}

```

```

G1[v_,g_]:= G[v[[1]],v[[2]],v[[3]],g]

```

```

Gp[x_,g_]:= Block[{},Glist=Table[0,{z,10}]; Do[Glist[[Floor[i/5
+1]]]=G1[tv[[i]],g],{i,1,x,5}]]

```

```

Gf:=Drop[Glist,-Count[Glist,0]]

```

(* The following functions calculate the position of each joint for
the graphics functions. *)

$x_1[t_1] := \cos[t_1]$

$y_1[t_1] := \sin[t_1]$

$x_2[t_1, t_2] := x_1[t_1] + \cos[t_1 + t_2]$

$y_2[t_1, t_2] := y_1[t_1] + \sin[t_1 + t_2]$

$x_3[t_1, t_2, t_3] := x_2[t_1, t_2] + \cos[t_1 + t_2 + t_3]$

$y_3[t_1, t_2, t_3] := y_2[t_1, t_2] + \sin[t_1 + t_2 + t_3]$

Bibliography

1. S. Hirose and Y. Umetani. *The Basic Motion Regulation System for a Quadruped Walking Machine*. ASME Paper 80-DET-34. 1980.
2. K.J. Waldron and G.L. Kinzel. The Relationship Between Actuator Geometry and Mechanical Efficiency in Robots. *Proceedings of 4th CISM IFToMM Symp. Theory and Practice Robots and Manipulators*. Amsterdam: Elsevier, pp. 366-374. Zabrow, Poland, 1981.
3. Shin-Min Song and Jong-Kil Lee. The Mechanical Efficiency and Kinematics of Pantograph Type Manipulators. In *Proceedings of the IEEE International Conference on Robotics and Automation*, pages 414-420. April 1988.
4. C.H. Spenny and M.P. Leahy, Jr. Geometric Mechanical Efficiency: A Metric for Selecting Manipulator Kinematic Structure. In *Issues in the Modeling and Control of Biomechanical Systems*, pages 71-77. Winter Annual Meeting of the ASME. 1989. Volume 17.
5. T. Yoshikawa. Analysis and Control of Robot Manipulators with Redundancy. In *Robotics Research*, eds. M. Brady and R. Paul, pp. 735-747. The MIT Press. Cambridge, MA, 1984.
6. J.K. Salisbury and J.T. Craig. Articulated Hands: Force Control and Kinematic Issues. *The International Journal of Robotics Research*, 1(1):4-17. 1982.
7. P. R. McAree, A. E. Samuel, K.H. Hunt, and C.G. Gibson. A Dexterity Measure for the Kinematic Control of a Multifinger, Multifreedom Robot Hand. *The International Journal of Robotics Research*, 10(5):439-452, October, 1991.
8. Yoshihiko Nakamura. *Advanced Robotics: Redundancy and Optimization*. Addison-Wesley Publishing Company. New York, 1991.
9. O. Bottema and B. Roth. *Theoretical Kinematics*. Amsterdam: North Holland. 1979.
10. Kenneth H. Hunt. *Kinematic Geometry of Mechanisms*. Clarendon Press, Oxford, 1978.
11. J.K. Salisbury and B. Roth. Kinematic and Force Analysis of Articulated Mechanical Hands. *Journal of Mechanisms, Transmissions, and Automation In Design*, pages 35-41. March 1983. Volume 105.
12. W. Holzmann and J. Michael McCarthy. Computing the Friction Forces Associated with a Three-Fingered Grasp. *IEEE Journal of Robotics and Automation*, RA-1(4): 206-210, December 1985.
13. M.S. Ohwovoriole and B. Roth. An Extension of Screw Theory. In *Transactions of the ASME, Journal of Mechanical Design*, pages 725-735. October 1981. Volume 103.

14. Wesley E. Snyder. *Industrial Robots: Computer Interfacing and Control*. Prentice-Hall, Inc., Englewood Cliffs, NJ, 1985.
15. Mikell P. Groover, Mitchell Weiss, Roger N. Nagel, and Nicholas G. Odrey. *Industrial Robotics: Technology, Programming, and Applications*. McGraw-Hill Book Company, New York, 1986.
16. Richard W. Jones. *Electric Control Systems*. John Wiley & Sons, Inc; New York, 1953.
17. N.N. Hanock. *Electric Power Utilization*. Sir Isaac Pitman and Sons, Ltd; London, 1967.
18. John Watton. *Fluid Power Systems: Modeling, Simulation, Analog and Micro-computer Control*. Prentice Hall, New York, 1989.
19. J. Michael McCarthy. *An Introduction to Theoretical Kinematics*. The MIT Press, Cambridge, MA, 1990.
20. Francis H. Raven. *Automatic Control Engineering*. McGraw-Hill Book Company, Inc., New York, 1961.
21. Mark W. Spong and M. Vidyasagar. *Robot Dynamics and Control*. John Wiley & Sons, Inc., New York, 1989.
22. Zexiang Li, Ping Hsu, and Shankar Sastry. Grasping and Coordinated Manipulation by a Multifingered Robot Hand. *The International Journal of Robotics Research*, 8(4):33-50, August, 1989.

Vita

Captain Nathan A. Titus was born on 3 February 1965 in Pontiac, Michigan. In 1982, he graduated from the Vocational High School Division of Guam Community College in Mangilao, Guam. He then attended the University of Washington on a ROTC scholarship. He received a degree of Bachelor of Science in Aeronautical and Astronautical Engineering and an Air Force commission in June 1986. In November of that year, he was assigned to the Air Force Satellite Control Facility, OL-AB, in Colorado Springs, CO. While awaiting training, he was temporarily given duties at Headquarters AFSPACECOM, in the Space Defense Plans (XPDD) office. He was then trained as a Planner/Analyst for the Fleet Satellite Communications (FLT-SATCOM) program, and was a member of the team that activated the 3rd Satellite Control Squadron. He entered the Air Force Institute of Technology in June 1991. Upon receiving his master's degree in Astronautical Engineering in December 1992, Captain Titus will be assigned to the Phillips Laboratory, Kirtland AFB, NM.

Permanent address: 15310 Washington Ave SW
Tacoma, WA 98498

100

4. 11. 2 5. 10 6. 9 7. 8 8. 7 9. 6 10. 5 11. 4 12. 3 13. 2 14. 1

5. 4. 1. 2. 3. 4. 5.

1. *Journal of the American Medical Association*, 1997; 278: 1039-1044.

AFIT/GA/ENY/92D-12

© 2006 The Authors
Journal compilation © 2006 Blackwell Publishing Ltd

1. The first step in the process is to identify the problem or issue that needs to be addressed. This involves gathering information and understanding the context of the problem.

13. ABSTRACT Maximum 200 words)

14. SUBJECT TERMS

15. NUMBER OF PAGES

97

5, 22, 23, 233

19. SECURITY CLASSIFICATION
OF ABSTRACT
Unclassified

UL